THE ASTROPHYSICAL JOURNAL, 287:633–652, 1984 December 15

SAS 3 SURVEY OF THE SOFT X-RAY BACKGROUND[1]

FREDERIC J. MARSHALL AND GEORGE W. CLARK
Center for Space Research and Department of Physics, Massachusetts Institute of Technology
Received 1984 March 30; accepted 1984 June 25

ABSTRACT

We report the results of a survey of the soft X-ray sky in the *C* band (0.10–0.28 keV) which provides evidence for a nonlocal origin of a substantial portion of the low-energy X-ray background. The survey, compiled from data obtained with the *SAS 3* X-ray observatory, covers 80% of the sky with an angular resolution of 2°.9 FWHM and a total exposure of 2.2×10^4 cm^2 s sr. We find that *C* band counting rates are generally anticorrelated with the column density of neutral hydrogen, on all angular scales down to the angular resolution of our detector. In the octant of the sky defined by $90° < l < 180°$, $0° < b < 90°$, which is comparatively free of conspicuous local enhancements in the soft X-ray intensity, the relation between the *C* band rates and the column densities of neutral hydrogen can be fitted, with a residual rms deviation of less than 13%, by a two-component model of the X-ray background in which the expectation value of the *C* band rate is expressed by the formula $c' = C_1 + C_2 \exp(-N_{av}/N_{ap})$, where N_{av} is the mean column density in the field of view. We attribute the constant component, C_1, to *X*-rays with an energy flux in the *C* band of 1.4×10^{-8} ergs cm^{-2} s^{-1} sr^{-1} generated in a local region ($D \lesssim 100$ pc) of hot plasma within which the solar system is located. We attribute the variable component, $C_2 \exp(-N_{av}/N_{ap})$, to X-rays generated in a region external to the neutral hydrogen of the galactic disk and having an energy flux in the *C* band of 3.1×10^{-8} ergs cm^{-2} s^{-1} sr^{-1} before attenuation by photoelectric absorption in the interstellar medium. For N_{ap}, the apparent attenuation column density, we find a value of 2.7×10^{20} cm^{-2}, which is about twice the expected value for photoelectric absorption of *C* band X-rays in neutral gas with $N_{He}/N_H = 0.085$. From a computer simulation study we find that the explanation of this anomaly as an effect of the clumping of interstellar matter is consistent with the magnitude of the spatial fluctuations in the *C* band map and other information about the interstellar medium. We attribute most of the external component to emission from a galactic corona with a luminosity in the *C* band of about 5.4×10^{39} ergs s^{-1}. When the background rates, calculated from the two-component formula, are subtracted from the survey map, the resulting "flattened" map shows foreground emission and absorption features with improved sensitivity and clarity.

Subject headings: galaxies: Milky Way — galaxies: structure — X-rays: sources

I. INTRODUCTION

Observations by Bowyer, Field, and Mack (1968), Bunner *et al.* (1969), Davidsen *et al.* (1972), and by others (see review by Tanaka and Bleeker 1977 and references therein) established the existence of a soft X-ray background (XRB) which is highly anisotropic and more intense in all directions than would be predicted by an extrapolation of a power law that fits the spectrum of the XRB in the energy range from 2 to 10 keV. Intensities in the energy range from 0.10 to 0.28 keV, which we designate the *C* band, are found to be generally anticorrelated with the column densities of galactic neutral hydrogen. However, in directions of very large column densities the intensity does not fall below about one-third of the maximum values observed in directions of very low column densities. A substantial portion of the *C* band XRB must therefore originate locally in a source or sources lying in front of this matter. Detailed assessment of the contribution of unresolved stars shows it to be less than 3% (Rosner *et al.* 1981). Thus it appears that the source of the local component of the *C* band XRB must be hot plasma in a region surrounding the solar system, a local "hot bubble." On the other hand, negative results from attempts to detect absorption due to diffuse matter in nearby extralgalactic objects (McCammon *et al.* 1971, 1976; Long, Agrawal, and Garmire 1976) have led to the conclusion that the fraction of the soft XRB produced in distant extragalactic sources is not more than a few percent. Thus the origin of any nonlocal component of the *C* band XRB must be in the Galaxy, e.g., the galactic halo.

If the anticorrelation between the count rates of a *C* band X-ray detector and the average values of the galactic neutral hydrogen column density over the fields of view of the detector is interpreted as an effect of interstellar absorption on a component from sources beyond the neutral hydrogen, then the apparent attenuation column density in the interstellar gas is found to be substantially larger and less dependent on energy than expected theoretically for absorption by uniform layers of neutral gas with normal cosmic abundances. Bowyer and Field (1969) and Bunner *et al.* (1969) pointed out that clumping of interstellar matter in X-ray thick clouds that subtend angles smaller than the angular diameter of the X-ray detector field of view would cause an increase in the apparent attenuation column density. Clumping would also cause a decrease in the energy dependence of the attenuation. Although some degree of clumping is now well established by 21 cm radio surveys of the neutral hydrogen and by optical studies of interstellar absorption lines and reddening, there remains doubt as to whether the apparent absorption anomaly can be consistently explained in this way, and therefore whether the idea of a

[1] This research was sponsored in part by a grant from the National Aeronautics and Space Administration under Contract NAS5-24441.

nonlocal origin for a substantial portion of the soft XRB is tenable (McCammon *et al.* 1983). An alternative "displacement" model has been put forward by Sanders *et al.* (1977) whereby all of the soft XRB is assumed to originate within a local hot bubble which has a highly convoluted boundary. In those directions where the boundary is closer, the emission measure of the X-ray producing plasma is smaller and the column density of the interstellar neutral hydrogen is correspondingly larger.

We have compiled a survey of the soft X-ray sky in the *C* band from data obtained with the low-energy detector system of the *SAS 3* satellite. The survey covers 80% of the sky with a higher angular resolution and larger exposure than has been previously available. In this paper we present the survey and use it as a basis for reexamining the origin and propagation of the soft X-ray background.

II. OBSERVATIONS AND DATA PROCESSING

a) Detectors

The *SAS 3* low-energy X-ray detector system has been described by Hearn *et al.* (1976). In brief, it had two independent flow proportional counters each with two stretched polypropylene windows, 80 μg cm^{-2} thick and coated on the inside with 24 μg cm^{-2} of colloidal graphite. Each of the four windows was at the focus of a grazing-incidence paraboloidal concentrator made of nickel-coated glass. A wheel with various filters, gold shutters, and open apertures was located between the concentrators and the detectors. For this survey we used only the data obtained with the larger open apertures which defined a field of view with an angular diameter of 2°.9 FWHM and an effective solid angle of 2.08×10^{-3} sr. Data obtained with the smaller apertures and the filters were too sparse to be useful. The proportional counters were connected to small tanks of liquid propane through pressure regulators that maintained the pressures constant at 1.09 atm to within about 1%. We determined how the gain varied with temperature from laboratory and in-flight calibration measurements of the distribution in height of pulses produced by fluorescent Al Kα radiation excited by an ^{55}Fe source.

Figure 1 shows plots of the effective areas as functions of energy for the pulse height channel corresponding to the *C* band at detector temperatures of $-10°$, 0°, and $+10°$C. We calculated the response of the detectors at 0°C to radiation produced by optically thin plasmas attenuated by passage through interstellar matter, using the theoretical spectra of Raymond and Smith (1977, 1979) for a thin plasma and the absorption cross sections of Brown and Gould (1970), both with a relative helium abundance of $n(\mathrm{He})/n(\mathrm{H}) = 0.085$. The results are shown in Figure 2*a* as plots of $R_c(T, N_\mathrm{H})$, the count rate per unit emission measure versus N_H, the column density, for three source temperatures. Figure 2*b* shows the energy flux per unit count rate both in the *C* band energy range and over the wide spectrum from 0.04 to 6.44 keV.

By calculating the detector responses at various operating temperatures, we obtained limits on the possible variations in count rate due to temperature variations in orbit. For source temperatures above 10^6 K the *C* band response varied by less than 10% over the range ($-10°$ to $+10°$C) of detector temperatures from which survey data were accepted. In compiling the survey data we made no corrections to the *C* band rates for variations of the detector temperature.

The satellite was launched by a Scout rocket on 1975 May 8 from the San Marco Platform off the coast of Kenya into a nearly circular orbit with an initial mean altitude of 513 km and an inclination of 3°.0, a situation that resulted in nearly the least possible interference from auroral and trapped particles that can be attained for a long-lived satellite observatory in near-Earth orbit.

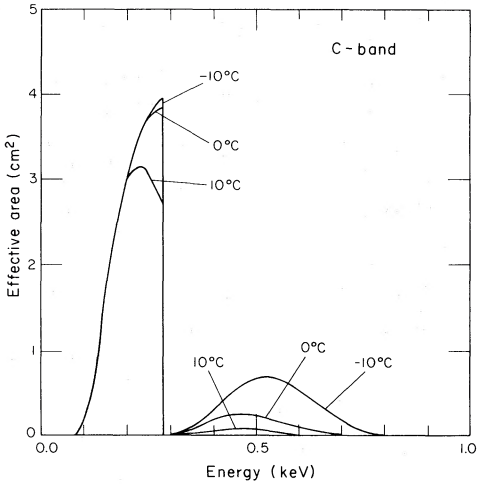

FIG. 1.—Effective areas vs. energy for the *C* band pulse height channel at detector temperatures of $-10°$, 0°, and $+10°$C.

b) Data Processing

The survey was carried out between 1975 May and 1976 November, mostly during periods when the satellite was rotating at a rate of one revolution per orbit. The data were packaged in units corresponding to one minor telemetry frame. Each unit contained the numbers of counts recorded separately in each of two energy channels from each of the two counters during 0.821 s, the celestial orientation of the detector axis to an accuracy of 0°.5 or better, and information about the configuration of the detector system.

Units of data were selected or rejected for inclusion in the survey according to criteria placed on the position in orbit, the orientation with respect to Earth, Sun, and Moon, and the conditions of operation. Data taken in sunlight when the detectors were pointed within 90° of the Sun were rejected to avoid contamination by solar UV and X-rays striking the inside of the concentrator and scattering into the counters. Data taken when the detectors were pointed within 90° of Earth's center were rejected on account of Earth blockage and solar UV and X-rays scattered from Earth's upper atmosphere. Data taken when the Moon was in the field of view were rejected because the Moon was a detectable source of scattered solar UV. Data taken near or in the South Atlantic anomaly were rejected on account of charged particle contamination. Data for this survey were accepted from only one of the two counters because the other one failed before the survey was half complete and was not in operation for much of the time before it failed. Data were accepted for mapping only when the open aperture of the filter wheel was in place.

The rates of particle-induced background counts, measured when the apertures were blocked by the gold shutters, averaged 0.035 s^{-1}, and varied by about 15% over typical orbits, excluding the region of the South Atlantic anomaly. No corrections were made for these small variations.

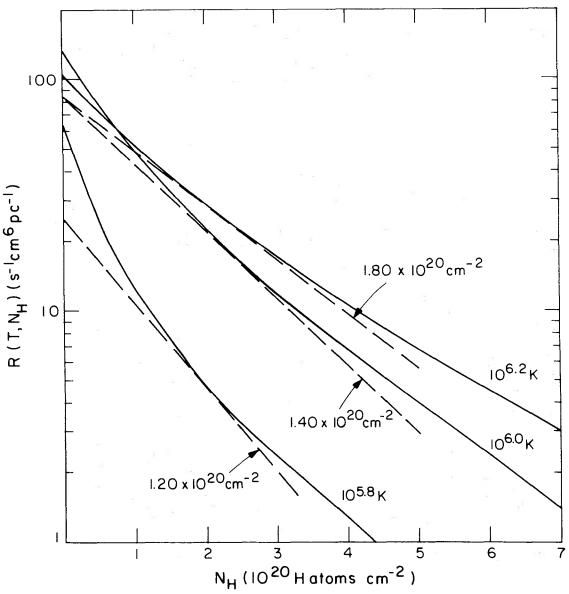

FIG. 2a

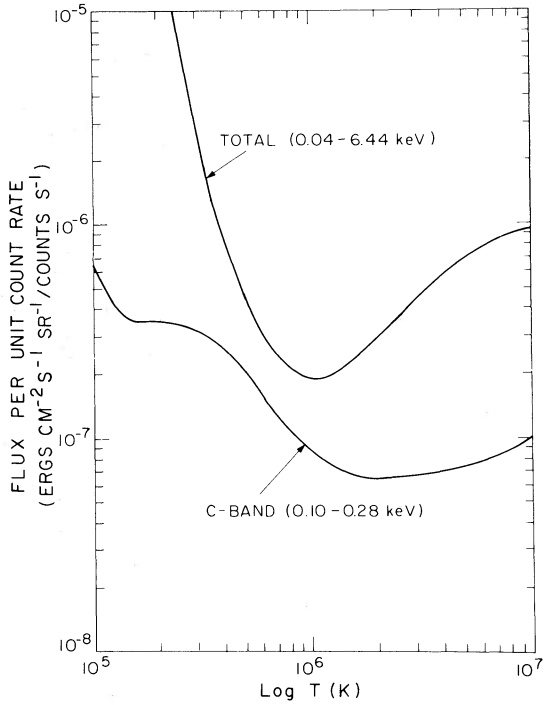

FIG. 2b

FIG. 2.—(*a*) Count rate per unit emission measure vs. column density of neutral hydrogen for three source temperatures. (*b*) Energy flux per unit count rate both in the *C* band energy range (0.10–0.28 keV) and over the entire spectrum.

A master X-ray map file was compiled in a series of steps that began at the level of one orbit of data. We first extracted the count and exposure from each unit of data that passed the selection criteria described above, and labeled the extracted data with a pair of map cell indices. These were compiled into the master X-ray map file in a stepwise procedure that facilitated a detailed examination of intermediate results and the identification of the causes of artifacts, which we gradually eliminated in reruns by tightening the various selection criteria to the ones specified above. The master map file was a 360 × 180 array of data cells corresponding to square elements of equal solid angle in a rectangular grid laid over an Aitoff projection of the sky centered at $(l, b) = (0°, 0°)$ with 0.81 deg^2 cells. Each data cell contained the total count and total exposure recorded while the axis of the detector was within the corresponding sky cell. (Data cells in the rectangular array outside the oval boundary of the Aitoff map were, of course, empty.) The master map file constituted the processed data base from which we prepared various projected map files with 3.24 deg^2 cells.

For statistical and correlation analyses we compressed the data of the master map file into a 180 × 90 rectangular array of data cells laid over an Aitoff projection with 3.24 deg^2 cells. Figure 3 is a map of the exposure times in this compressed map file. Figure 4 is a plot of the fraction of 3.24 deg^2 skycells which received exposure times equal to a given amount or more as a function of exposure time. The total time is 2.7×10^6 s, and the total exposure is 2.2×10^4 cm^2 s sr.

Each *C* band count rate display map was prepared from a map file with 3.24 deg^2 cells by a two-pass smoothing process. In the first pass the count and exposure in each map cell were replaced by the weighted means of counts and exposures in the 3 × 3 array centered on that cell. In the second pass the count and exposure of each cell were replaced by the count and exposure of the cell with the medium counting rate of the 3 × 3 array centered on that cell (Frieden 1976). The purpose of the smoothing was to suppress statistical noise in areas of low exposure and to fill in small exposure holes while preserving sharp gradients. As a result, small-scale structure in the contours were suppressed, but features as large as or larger than the angular resolution of the detectors were preserved. The procedure degraded the angular resolution of the display maps from 2°.9 to about 4°.5 (FWHM). Areas with total exposure of less than 10 s were left blank.

In Figure 5 we display the *C* band rates in four projections so that each of the many complex features can be seen in a nearly flat representation in one or another of the maps. Figures 5*a* and 5*b* are Aitoff projections centered on the galactic center and anticenter, respectively. Figures 5*c* and 5*d* are Lambert azimuthal (polar) projections of the north and south galactic hemispheres respectively.

The master N_H map file was compiled from the recent survey of 21 cm line emission, in the velocity range (−100 to +100 km s^{-1}) with a resolution of 2°.0 (FWHM), carried out with the Bell Telephone Laboratory (BTL) microwave horn antenna by Stark *et al.* (1984). It covers the entire sky except the region below the BTL horizon which lies inside the small circle of radius 47° centered on galactic coordinates $(l, b) = (305°, -27°)$. The file contains the mean values of N_H in most of the 3.24 deg^2 cells of the X-ray map shown in Figure 5*a*. Figure 6 is a display map of the N_H data in which isolated cells for which survey data were not available were filled in with the average of the adjacent cells, and the region below the horizon was filled in with data, where available, from the Parkes survey (Heiles and Cleary 1979; Cleary, Heiles, and Haslam 1979). Since the Parkes survey did not contain data in the region of the sky

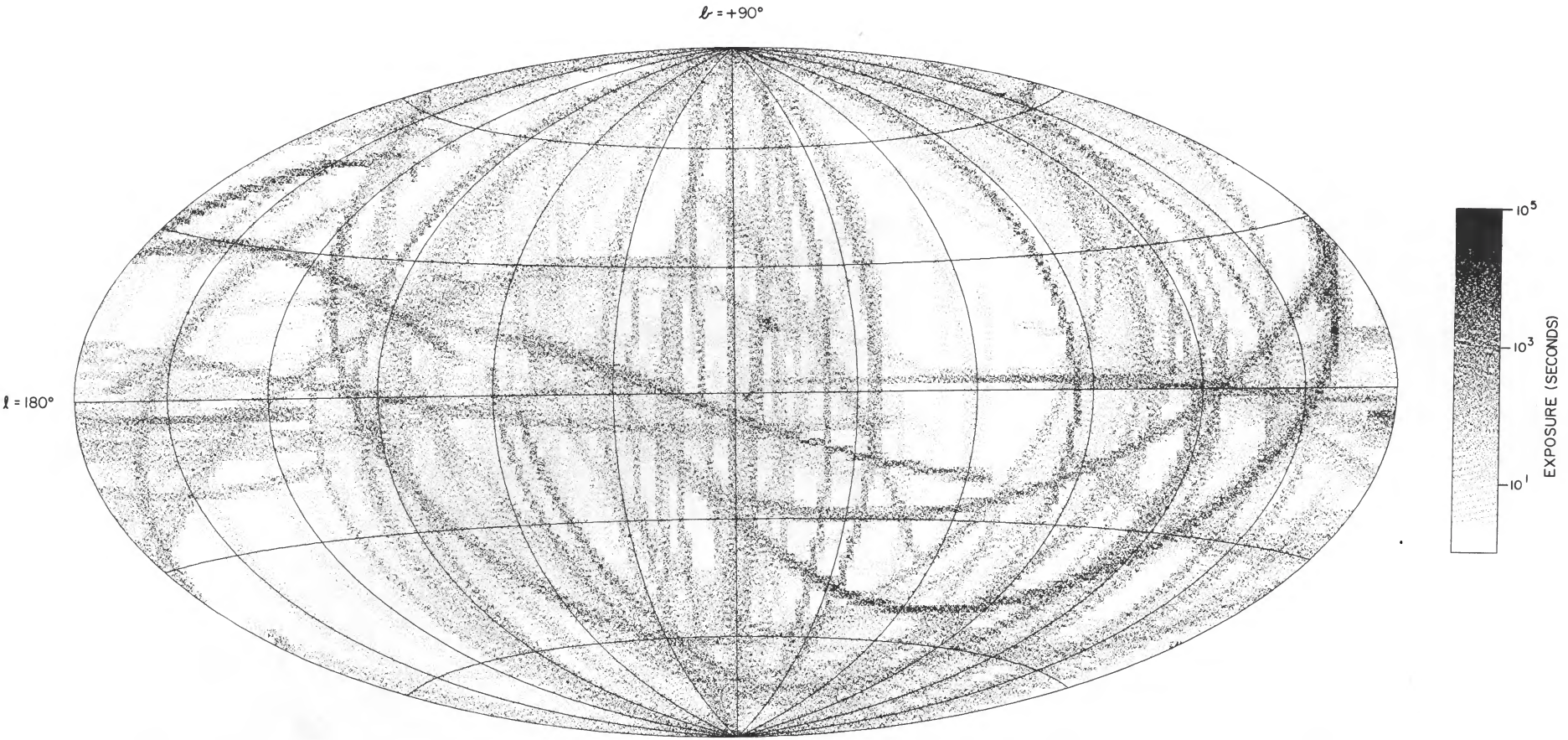

FIG. 3.—Map showing the distribution of exposure over the sky in an Aitoff projection of galactic coordinates

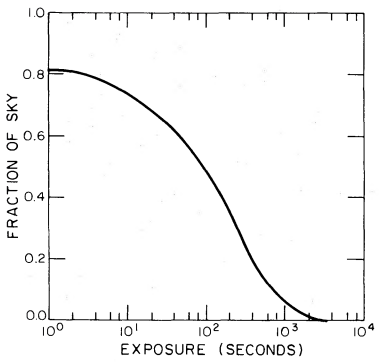

FIG. 4.—Fraction of 3.24 deg^2 sky cells with more than a given exposure vs. exposure. The total exposure of the accepted portion of the survey data is 2.7×10^6 s.

where $|b| < 10°$, we have displayed this region as having a column density, $N_H > 1 \times 10^{21}$ cm^{-2}. The display map has been smoothed to a resolution of $\sim 3°$ (FWHM).

To aid in visual comparison of the X-ray and neutral hydrogen data we show color maps of the *C* band rates and column densities in Figure 7 (Plate 8).

III. RESULTS AND ANALYSIS

a) C Band Maps

Previously described discrete sources (Gorenstein and Tucker 1976; Tanaka and Bleeker 1977; Nugent *et al.* 1983; Hearn, Marshall, and Jernigan 1979; and references therein) which are prominent in the *C* band maps include the Cygnus Loop at $(l, b) = (75°, -10°)$, the Vela SNR at (263°, −2°), the transient X-ray source A0620+00 at (210°, −6°), the hot white dwarf HZ 43 at (60°, 83°), Mkn 421 at (180°, 65°), and Capella at (165°, 4°). In addition, we have found a previously unreported and possibly variable source at (116°, 48°) which we designate MX 1335+683, and for which we suggest an identification with the Seyfert galaxy Mkn 270. Table 1 is a list of all the candidate sources we found by use of an algorithm which selected those map cells whose counting rates were more than 3 σ above the mean background level in the surrounding cells.

The most striking overall characteristic of the soft X-ray sky, clearly visible in these maps, is the general rise in intensity from the equator to the poles. This trend, as is well known, is opposite to that of the column density of neutral hydrogen.

Superposed on the general equator-to-pole trend are a number of previously reported extended soft X-ray enhancements (Tanaka and Bleeker 1977 and references therein) which include the Monoceros-Gemini enhancement centered at (205°, 10°), two enhancements in Eridanus at (200°, −40°) and (240°, −40°), the region known as the North Polar Spur extending from (30°, 30°) to (300°, 75°), and the Lupus enhancement around (320°, 25°) which appears more completely in the *C* band map of McCammon *et al.* (1983). We also call attention to the enhanced region which extends from (100°, 45°) to (135°, 70°), a region about 20° in diameter centered on (165°, 50°), a region with a count rate peak at (280°, 15°), and the large complex region extending from (240°, −50°) to (30°, −60°) all of which also appear in the maps of McCammon *et al.* (1983).

b) Correlation between the C Band and N_H Maps

Visual comparison of the *C* band and N_H maps (Figs. 5*a*, 6, and 7) shows that in many cases regions of low *C* band count rates (*C* rates) coincide with regions of high N_H values and regions of high *C* rates with regions of low N_H values. These coincidences are suggestive of "shadows" in the soft XRB due to foreground clouds.

On the level of visual comparison we note in particular the following features:

1. The 0.2 counts s^{-1} contour of the *C* band map, running from $(l, b) = (15°, 30°)$ to (330°, 45°) along the northern side of a broad region of low *C* rates, coincides with the 6×10^{20} cm^{-2} contour along the northern side of the region of high N_H associated with the Scorpius-Ophiuchus cloud complex lying at a distance of 200–300 pc. Two tongues of neutral hydrogen that extend out from the cloud complex near (340°, 50°) and (0°, 50°) are coincident with local dips in the *C* rates.

2. The ridge of high *C* rates running from (30°, 20°) to (0°, 80°) is the soft X-ray enhancement associated with the North Polar Spur (NPS). Adjacent to it is a valley of low *C* rates that coincides with a ridge of high N_H running northward from (35°, 20°) to (30°, 70°). Heiles *et al.* (1980) consider this ridge to be the limb brightened aspect of a neutral hydrogen shell with an average distance of 70 pc.

TABLE 1

DISCRETE C BAND SOURCES

	Location					
	Coordinates of Peak Bin		1950.0			
Source	l (deg)	b (deg)	α	δ	C Band Rate (s^{-1})	Identification
1	165.0	2.5	05^{h}11^{m}5	42°8	0.20 ± 0.06	Capella
2	182.7	−5.8	05 27.1	23.5	0.18 ± 0.06	Crab Nebula
3	209.0	−6.4	06 18.9	0.6	11.5 ± 0.3	Nova Mon 1975
4	260.5	−2.5	08 24.9	−42.4	5.0 ± 0.5	Vela SNR, Pup A
5	166.7	61.5	10 57.2	45.3	0.18 ± 0.06	AN UMa
6	178.1	64.6	11 0.8	39.3	0.26 ± 0.08	Mkn 421
7	53.0	83.2	13 18.4	29.5	1.30 ± 0.06	HZ 43
8	116.6	48.5	13 35.1	68.3	0.55 ± 0.09	Mkn 270
9	0.9	24.0	16 20.7	−14.1	0.44 ± 0.06	Sco X-1
10	77.2	26.7	18 9.2	49.4	0.22 ± 0.07	AM Her
11	336.2	32.5	20 2.0	−60.8	0.20 ± 0.05	H2001–60
12	75.0	−8.0	20 49.8	31.6	8.0 ± 0.3	Cygnus Loop

PLATE 8

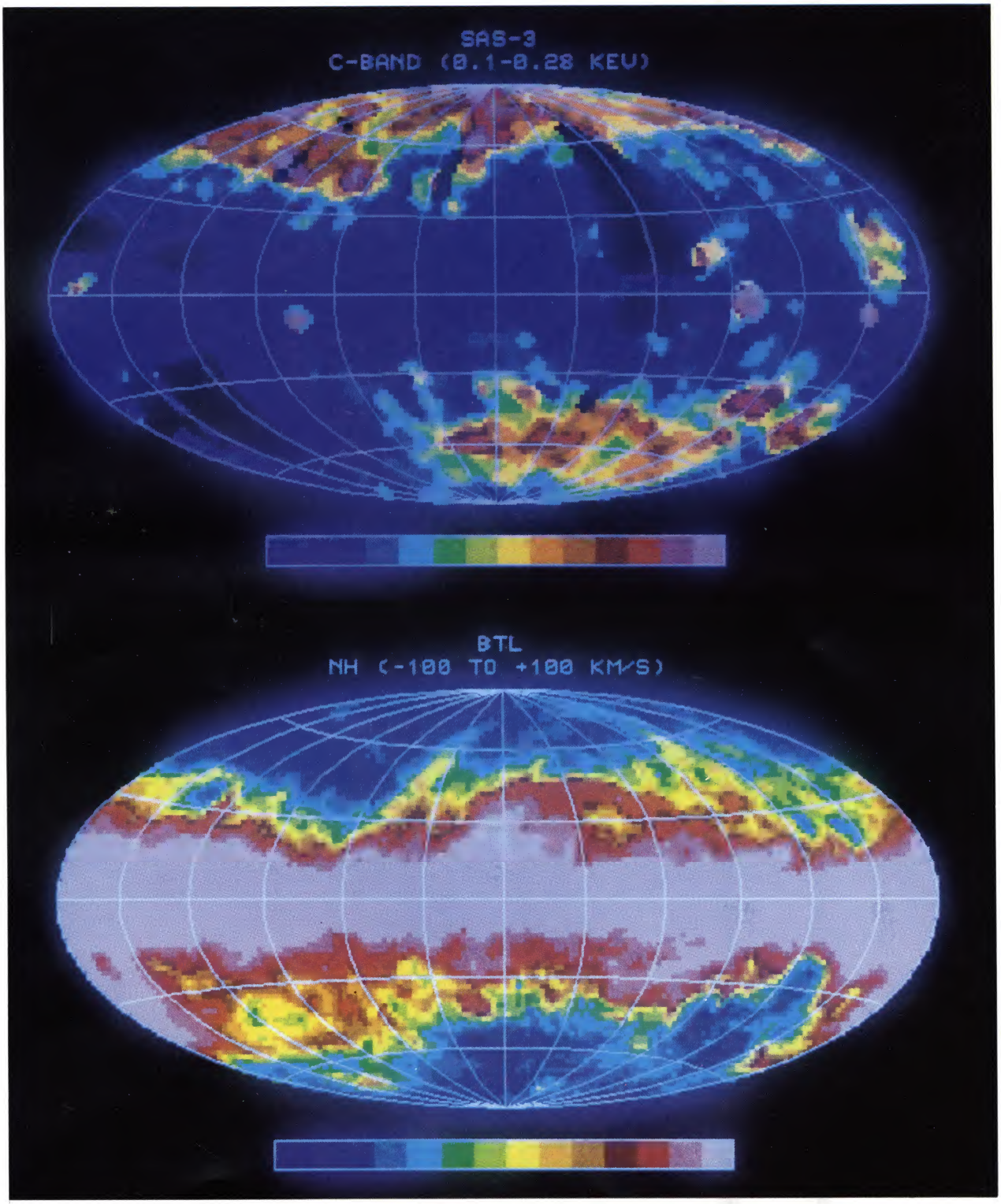

FIG. 7.—False color maps of (*a*) the *SAS 3 C* band soft X-ray survey and (*b*) the neutral hydrogen survey carried out with the Bell Telephone Laboratory (BTL) horn antenna (Stark *et al.* 1984). in Fig. 7*b* the region below the BTL horizon is filled with data from the Parkes survey (Heiles and Cleary 1979; Cleary, Heiles, and Haslam 1979).

MARSHALL AND CLARK (*see* page 637)

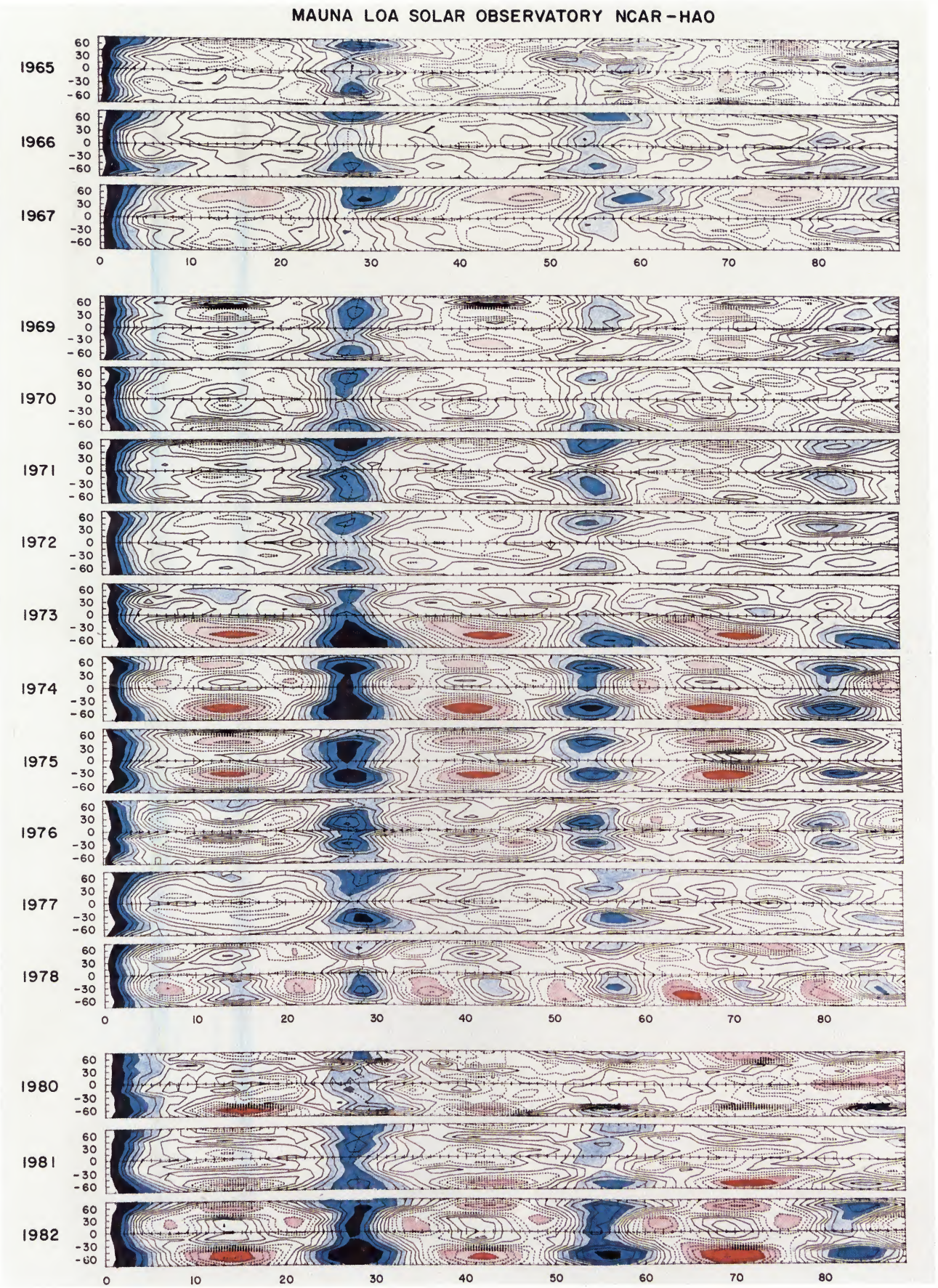

FIG. 11.—Autocorrelation surfaces from the Mauna Loa K-coronameters for the period 1965–1983, from which the synodic rotation periods of Fig. 4 were estimated. The contour interval is 0.1; negative values are indicated with dashed contour lines. The color code for the amplitude of the correlation coefficient is given in the Appendix.

FISHER AND SIME (*see* page 637)

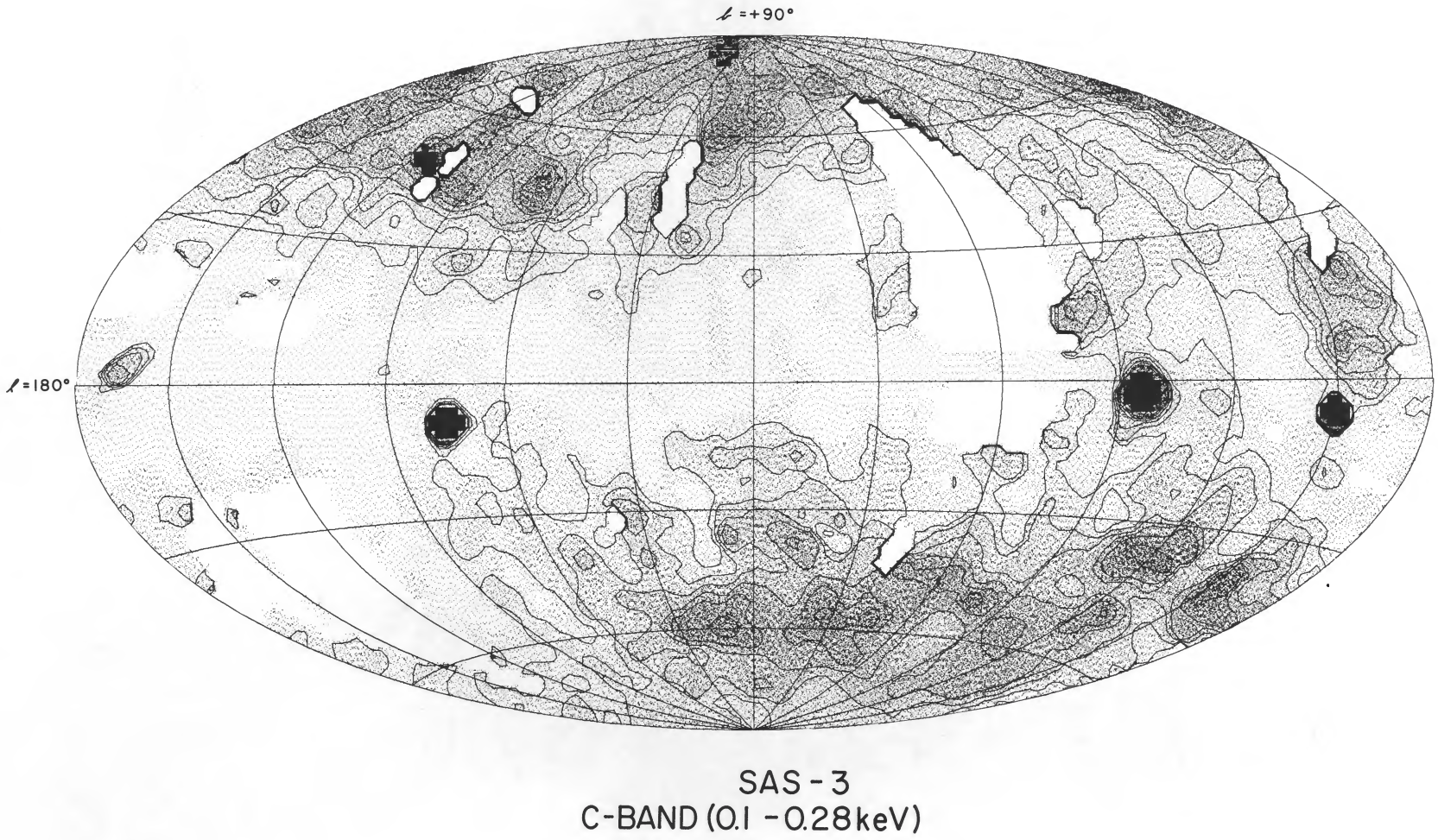

FIG. 5a

FIG. 5.—Maps of the *C* band count rates in various projections of galactic coordinates. Contours are at 0.20, 0.25, 0.30, 0.35, 0.40, and 0.45 counts s^{-1}. (*a*) Aitoff projection centered on $(l, b) = (0°, 0°)$. (*b*) Aitoff projection centered on $(l, b) = (180°, 0°)$. (*c*) Lambert azimuthal projection centered on the north galactic pole. (*d*) Lambert azimuthal projection centered on the south galactic pole.

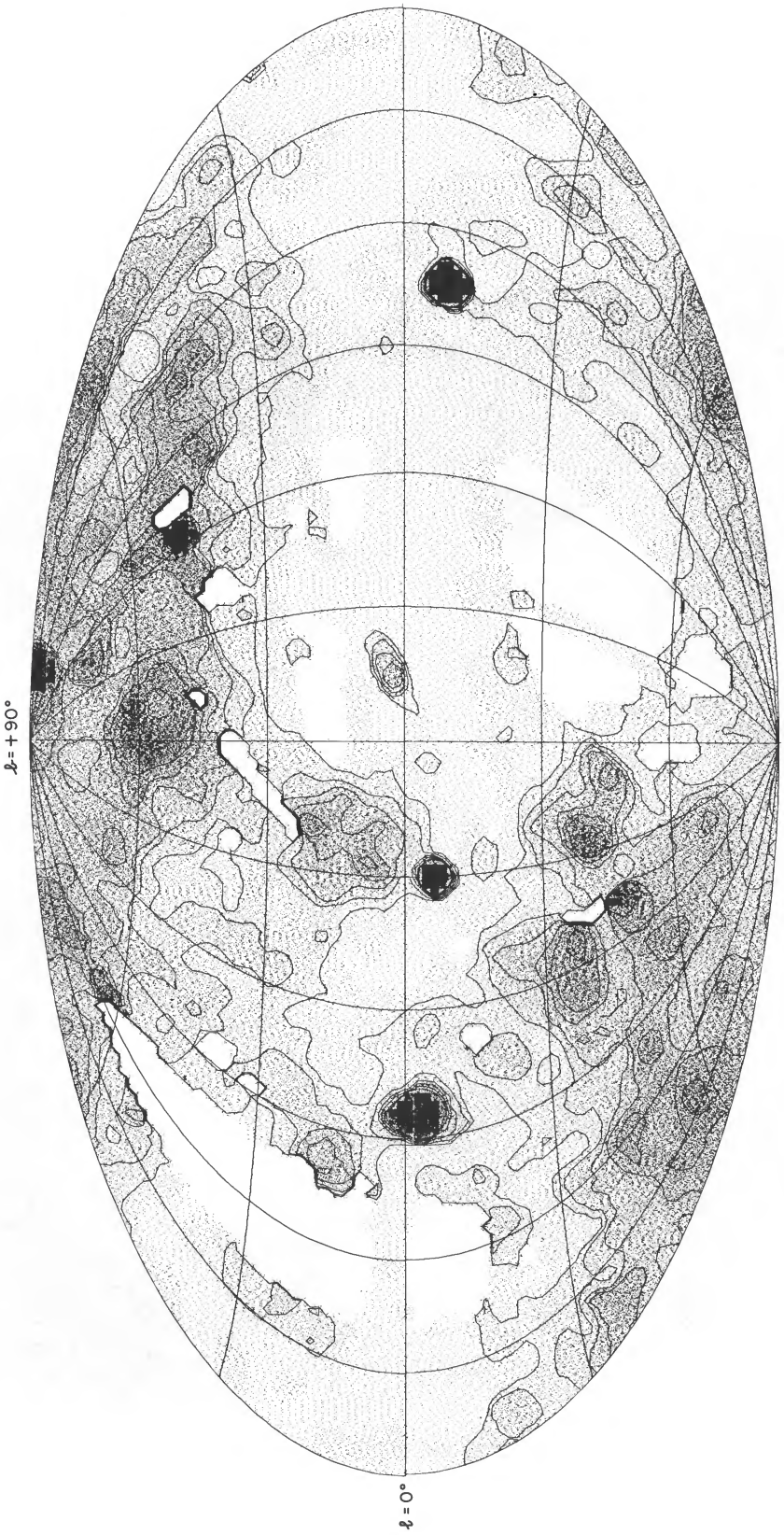

FIG. 5b

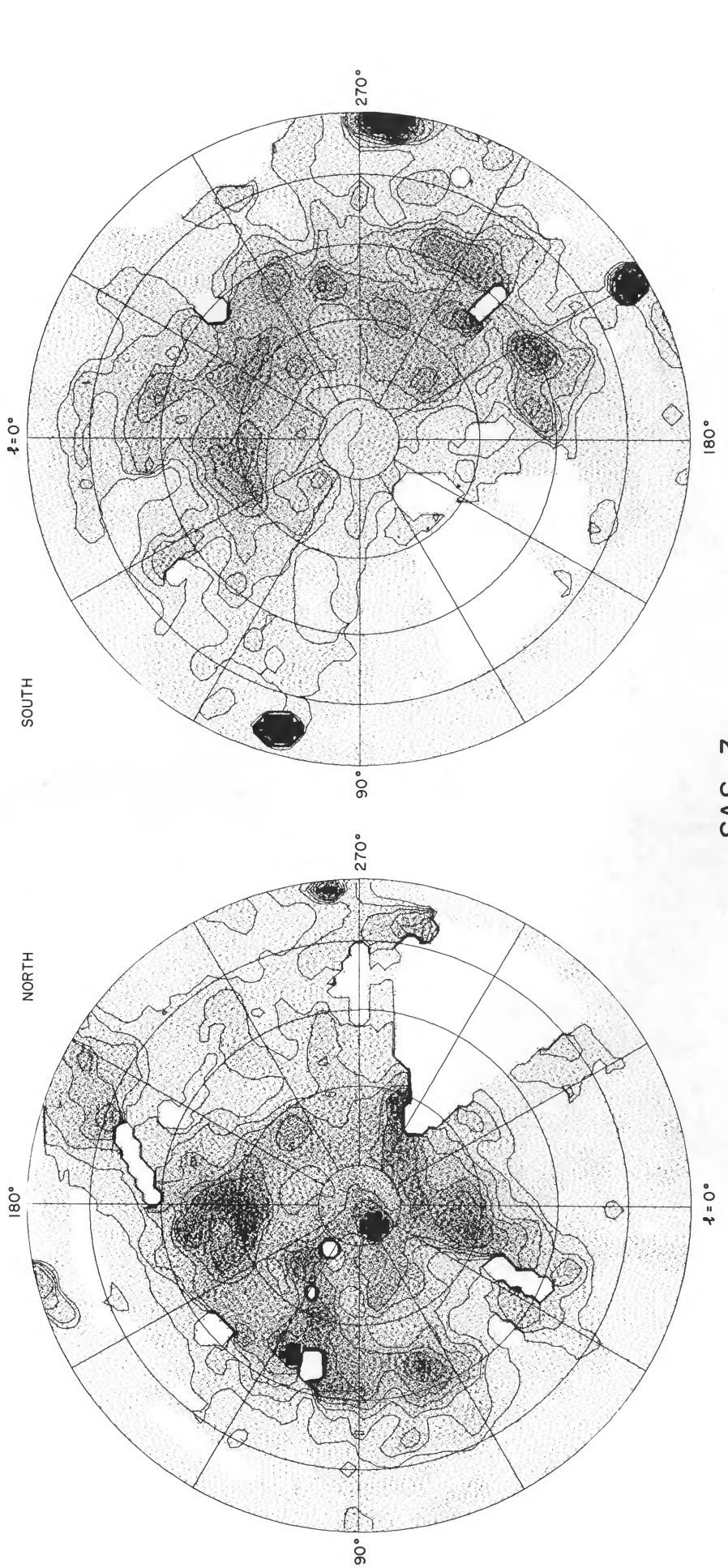

FIG. 5d

FIG. 5c

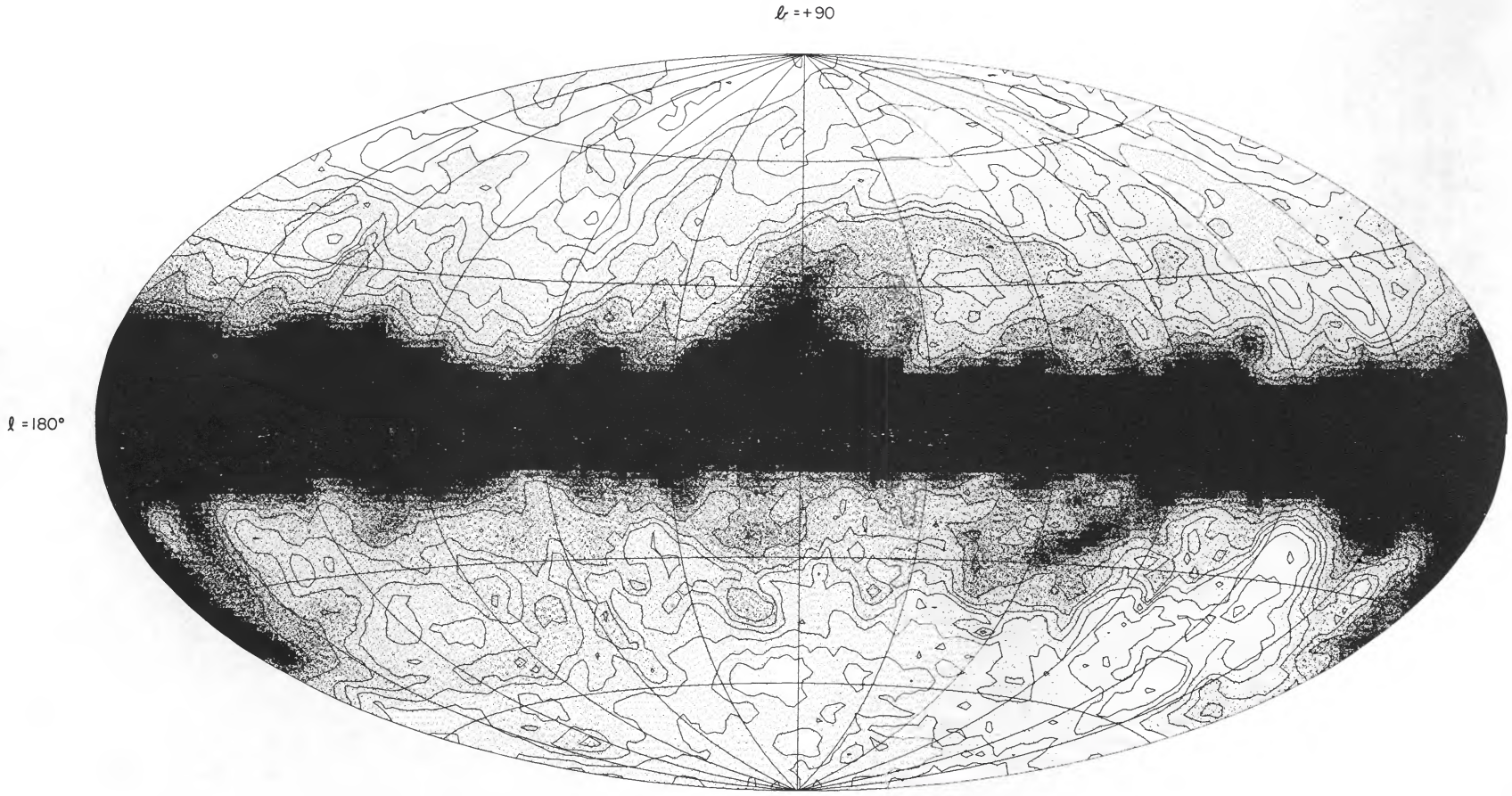

FIG. 6.—Map of the column densities of neutral hydrogen derived from the BTL survey of Stark *et al.* (1984). The region below the BTL horizon is filled with data from the Parkes survey (Heiles and Cleary 1979; Cleary, Heiles, and Haslam 1979). Contours are at 1.0, 1.5, 2.0, 3.0, 4.0, 5.0, 6.0, 8.0, and 10.0 in units of 10^{20} H atoms cm^{-2}.

3. The enhancement at (70°, 45°), previously reported by Clark (1975) as MX 1640+40 and Iwan (1980) as the Hercules hot spot, coincides with a deep hole in the neutral hydrogen column density ($N_H \lesssim 1 \times 10^{20}$ cm^{-2}).

4. An elongated feature in the distribution of high-latitude neutral hydrogen in which $N_H > 1.5 \times 10^{20}$ cm^{-2} running from (60°, 50°) over to (90°, 60°) and then up to (180°, 75°) coincides with a similarly shaped region of relatively low C rates as compared to the surround.

5. A small island of higher C rates centered near (135°, 35°) coincides with the central depression of a 20° diameter N_H loop which Hu (1981) has identified as an expanding H I shell at a distance of 334 pc.

6. The C rates are higher north of the $N_H = 2 \times 10^{20}$ cm^{-2} contour which runs from (180°, 42°) up to (240°, 60°).

7. A ridge of neutral hydrogen extending from (330°, 40°) to (290°, 35°), within which $N_H > 6 \times 10^{20}$ cm^{-2}, coincides with a region of low C rates where *SAS 3* data exist. Weaver (1979) suggests that this feature is part of an expanding shell that may have been produced by stellar winds from the Sco-Cen OB association lying at a distance of about 200 pc.

8. Several fingers of high C rates, extending from high southern latitudes toward the equator, coincide with similarly shaped features of low N_H values, in particular from (30°, −50°) to (30°, −25°), from (50°, −60°) to (50°, −35°), from (195°, −35°) to (195°, −25°), and from (230°, −30°) to (230°, −15°).

9. Small anticorrelated features are located at (60°, −30°), (120°, −70°), (15°, −40°) and (340°, −35°).

10. The Eridanus enhancement centered near (205°, −40°) is surrounded by an expanding N_H shell (Heiles 1976) part of which coincides with the valley of low C rates extending from (195°, −55°) to (220°, −40°). The enhancement itself, inside the shell, is presumably emission from the hot gas of the supernova remnant which is pushing out the shell. The increase in C rates outside the shell, on the other side of the valley, coincides with a decrease in N_H.

An objective indicator of the spatial anticorrelation between the C band and N_H maps is shown in Figure 8. It is the spatial cross correlation function (CCF) in the mid-latitude range $30° < |b| < 60°$, plotted as a function of offset in galactic longitude. The values have been normalized by dividing them by the peak negative value, which occurs at zero offset. For purposes of comparison the normalized autocorrelation functions (ACF) of the X-ray and neutral hydrogen maps are also shown. The CCF peaks at zero offset, indicating a significant alignment of the patterns in the two maps. In fact, the CCF has nearly the same shape as the radio ACF with the exception of deviations near 60° which are apparently caused by large high latitude N_H features that are fortuitously aligned with large exposure gaps in the X-ray map at that offset. The X-ray ACF also is similar in shape to the CCF with the exception of the large spike at zero offset caused by Poisson noise. The fact that the shapes of the three correlation functions are similar suggests that correlated features dominate the soft X-ray and 21 cm skies at these latitudes.

Another objective indicator is the coefficient of linear correlation between the local fluctuations in the C band and N_H maps, which we define by

$$r = \langle (c_i - \bar{c}_i)(N_i - \bar{N}_i)\rangle / [\langle (c_i - \bar{c}_i)^2\rangle \langle (N_i - \bar{N}_i)^2\rangle]^{1/2} , \quad (1)$$

where c_i and N_i are the values in the ith map cell, $\bar{c}_i$ and $\bar{N}_i$ are the mean values in the eight cells surrounding the ith cell, and the symbol "$\langle\rangle$", denotes the mean value of the quantity enclosed. Because of exposure holes in the unsmoothed C band and N_H maps, the number of cells for which fluctuations can be derived in both maps is small compared to the total number of map cells. Nevertheless, enough are available to yield a broad sampling of the sky. The results are listed in Table 2 for each of three latitude bands in each of the seven octants well covered by the BTL survey. The probability that 16 or more would be negative if the count rate and column density fluctuations were uncorrelated is 0.013. In the midlatitude range, where the broad-scale anticorrelation is most conspicuous to the eye, all seven values are negative (probability <0.01), and three are such that the probabilities of their being exceeded are <0.04 if the fluctuations are uncorrelated. These results demonstrate the existence of anticorrelated spatial fluctuations in the mid-latitude regions on an angular scale of 2°.

To measure the magnitude of the small-scale fluctuations in the C band map we found the value of a quantity, F_x, defined implicitly by the equation

$$1.0 = \frac{1}{m} \sum_{i=1}^{m} \frac{(c_i - \bar{c}_i)^2}{\bar{c}_i/t_i + (1/64) \sum_{j=1}^{8} (\bar{c}_i/t_{ij}) + (F_x \bar{c}_i)^2} . \quad (2)$$

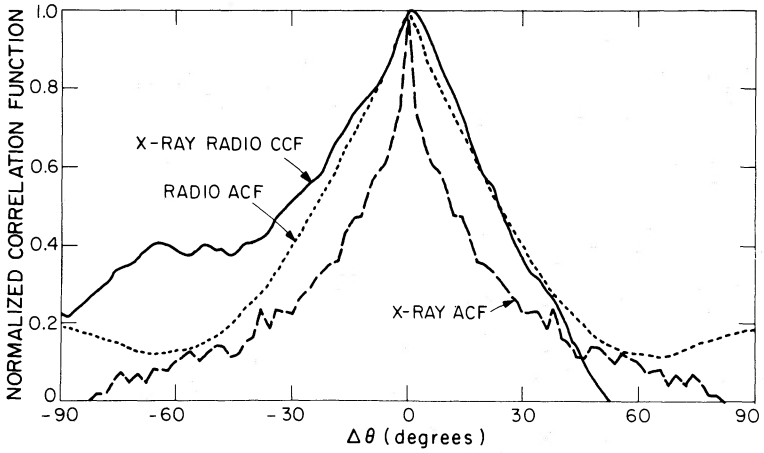

FIG. 8.—Spatial cross-correlation (CCF) and autocorrelation (ACF) functions of the X-ray and neutral hydrogen maps

TABLE 2

SMALL-SCALE (~2°) FLUCTUATIONS IN C AND N_H MAPS

Range	$180 > l > 90$			$90 > l > 0$			$360 > l > 270$			$270 > l > 180$		
$60° < b < 90°$	46	1.42E20	0.070	126	1.90E2	0.071	96	2.02E20	0.066	169	2.57E20	0.102
	69	0.432	0.087	44	0.450	0.055	52	0.435	0.065	50	0.384	0.034
	16	+0.23	0.39	34	−0.12	0.50	35	+0.14	0.42	48	−0.06	0.69
$20° < b < 60°$	514	5.59E20	0.076	547	5.08E20	0.071	472	6.61E20	0.077	653	4.67E20	0.087
	161	0.265	0.102	132	0.251	0.078	123	0.202	0.064	168	0.291	0.103
	149	−0.09	0.28	105	−0.21	0.032	93	−0.04	0.70	157	−0.19	0.017
$0° < b < 20°$	330	37.8E20	0.072	378	31.3E20	0.110	103	24.3E20	0.095	360	25.4E20	0.105
	121	0.183	0.090	193	0.174	0.070	42	0.176	0.078	146	0.267	0.060
	83	−0.004	0.98	161	+0.18	0.022	23	−0.25	0.25	138	+0.03	0.73
$-20° < b < 0°$	274	33.2E20	0.070	246	34.3E20	0.127	34	36.7E20	0.145	279	37.7E20	0.083
	235	0.172	0.105	251	0.186	0.109	79	0.224	0.113	177	0.226	0.093
	159	−0.07	0.38	128	−0.02	0.82	...	...	...	147	−0.04	0.63
$-60° < b < -20°$	233	7.88E20	0.067	204	6.11E20	0.064	...	...	...	288	7.04E20	0.091
	130	0.197	0.050	308	0.297	0.080	119	0.339	0.060	233	0.338	0.079
	32	−0.13	0.48	77	−0.32	0.004	...	...	...	106	−0.04	0.68
$-90° < b < -60°$	4	1.71E20	0.067	58	1.60E20	0.073	21	1.69E20	0.141	14	2.18E20	0.133
	86	0.264	0.106	146	0.371	0.066	126	0.412	0.049	129	0.382	0.0
	4	−.003	1.0	50	−0.18	0.21	...	...	...	12	+0.02	0.95

NOTE.—Key to entries: m_n N_H F_N
m_x C F_c
m_{xn} r p

m_n, m_x, m_{xn} = numbers of sky cells accepted; N_H = mean value of N_H; F_N = fractional fluctuations in N_H; C = mean count rate; F_c = fractional fluctuations in C; r = correlation coefficient; p = probability of value $\geq r$ for uncorrelated fluctuations.

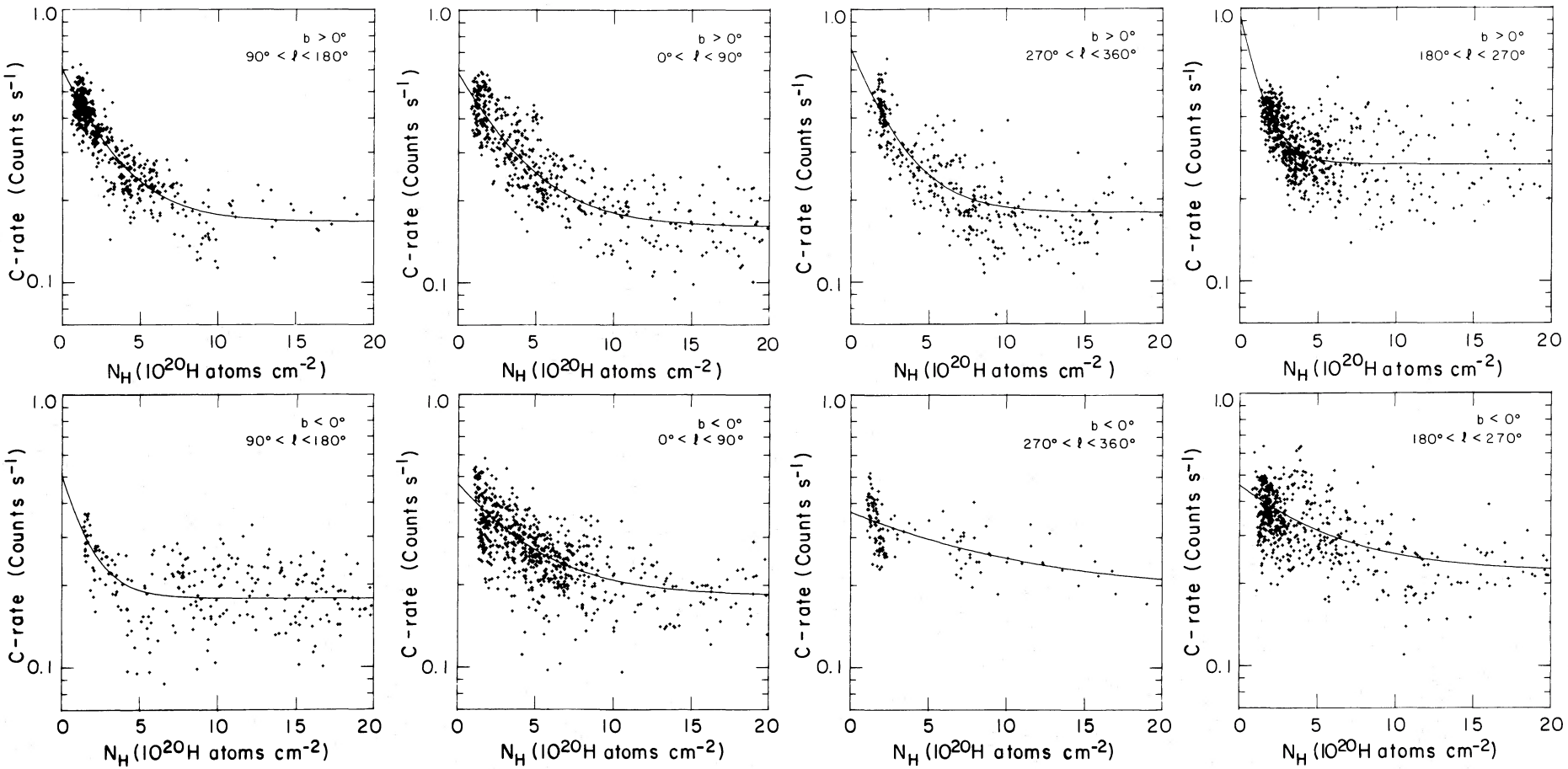

FIG. 9.—Semilog plots of count rates vs. column densities in eight octants of the sky. Each octant is the interior of a spherical triangle bounded by the galactic equator and two meridia separated by 90°.

In this formula c_i and t_i are the count rate and exposure in the ith cell, t_{ij} is the exposure in the jth cell of the eight surrounding cells, and $\bar{c}_i$ is the average rate in those eight cells. The first two terms in the denominator are an estimate of the contribution of Poisson fluctuations to the variance of $(c_i - \bar{c}_i)$—an estimate that would be optimal if the C band intensity were perfectly isotropic. The third term, containing the factor F_x, represents the contribution to the variance from spatial fluctuations in the intensity and measurement errors. All cells with at least 10 s of exposure were included. In Table 2 we list the number of cells included, the mean value of the count rate, and F_x in 24 regions. We note that in the midlatitude region the largest value of F_x is 0.103. A similar analysis was performed on the BTL column density data, but in this case the denominator was the sum of the variance due to baseline errors, which we assumed is $(1.0 \times 10^{19}\ \mathrm{cm}^{-2})^2$, and a term $(F_{\mathrm{H}} \bar{N}_i)^2$ representing the variance due to combined measurement and intrinsic fluctuations. The number of cells included, the mean value of the column density, and the fractional fluctuation are also listed in Table 2.

Figures 9*a*–9*h* are semilog plots of c_i versus N_i in the eight octants of the sky. In each octant the data run from the equator to the pole between meridia separated by 90°, and they include all sky cells from the unsmoothed 3.24 deg^2 map with more than 100 s of exposure and with centers lying more than 3° from any of the sources listed in Table 1. The count rates have not been corrected for the systematic contribution from particle-induced background which, as noted previously, amounts to (0.035 ± 0.010) counts s^{-1}. Uncertainties in the measurements are due principally to count statistics and are therefore 0.1 times the square root of the count rate or less. We note that the trend of the correlation between c_i and N_i is suggestive of a relation in which c_i is the sum of a constant plus an exponentially decreasing function of N_i. The smooth curves in Figures 9*a*–9*h* are the result of model fits discussed in the following section.

IV. INTERPRETATION

a) Two-Component Model of the Soft XRB

The basic question we wish to address is whether or not the anticorrelation of the C band and N_{H} maps is, in fact, caused by photoelectric absorption of a component of X-rays produced in sources beyond a local hot bubble. This idea obviously provides a plausible explanation for the apparent existence of "shadows" of foreground clouds and the behavior of the cross-correlation measures described in § III*b*. In an effort to cast further light on the question we have investigated how well a two-component model, like that introduced by Davidsen *et al.* (1972), can be fitted to our survey data and whether the parameters of the fitted model are compatible with current knowledge of the interstellar medium. In this model the intensity of the soft XRB at a given energy in a given direction is expressed by the formula

$$I = I_1 + I_2 \exp\,(-N_{\mathrm{H}}/N_{\mathrm{th}})\,, \tag{3}$$

where N_{H} is the column density of neutral hydrogen in the given direction and N_{th} is the attenuation column density for photoelectric absorption of X-rays of the given energy by interstellar gas. This formula is valid for the variety of situations in which the observed intensity is the sum of a part, $I_e \exp\,(-N_{\mathrm{H}}/N_{\mathrm{th}})$, due to external sources beyond the absorbing gas, a part, $I_d[1 - \exp\,(-N_{\mathrm{H}}/N_{\mathrm{th}})$, due to sources in the disk which are coextensive with the absorbing gas and distributed with a density proportional to that of the gas; and a part, I_l, due to local sources in front of the absorbing gas. From these definitions and equation (2), it follows that $I_1 = I_l + I_d$ and $I_2 = I_e - I_d$.

Detailed maps of N_{H} derived from high-resolution 21 cm surveys in a few small regions (e.g., Verschuur 1974) show variations on angular scales that are small compared to the width of our field of view. Therefore the observed counting rates must be compared with the expected values of the averaged intensity over the fields of view. Bowyer and Field (1969) showed that if the unevenness of N_{H} is due to the clumping of interstellar matter in clouds that subtend solid angles small compared to the field of view and that have a distribution of column densities such that $m(N_c)dN_c$ is the number of clouds with column densities between N_c and $N_c + dN_c$ along a line of sight, then the expectation value of the average transmission for X-rays of a given energy in a given field of view is exp $(-N_{\mathrm{av}}/N_{\mathrm{ap}}')$, where N_{av} is the average value of N_{H}, and N_{ap}', the apparent attenuation column density, is given by

$$N_{\mathrm{ap}}' = N_{\mathrm{th}} \frac{\int m(N_c) N_c/N_{\mathrm{th}}\, dN_c}{\int m(N_c)[1 - \exp\,(-N_c/N_{\mathrm{th}})] dN_c}\,. \tag{4}$$

We note that if all clouds were optically thin, i.e., $N_c/N_{\mathrm{th}} \ll 1$, then $N_{\mathrm{ap}}' = N_{\mathrm{th}}$. If they were all thick, then $N_{\mathrm{ap}}' = N_{\mathrm{cav}}$, where N_{cav} is the average cloud column density. If they were all of the same column density, N_c, we would have

$$N_{\mathrm{ap}}' = N_c/[1 - \exp\,(-N_c/N_{\mathrm{th}})]\,. \tag{5}$$

For simplicity we assume that I_1 and I_2 do not vary significantly over any given field of view. Then the expectation value of the average intensity, which we call I_{av}', is given by

$$I_{\mathrm{av}}' = I_1 + I_2 \exp\,(-N_{\mathrm{av}}/N_{\mathrm{ap}}')\,. \tag{6}$$

The expectation value of the observed count rate, which we call c', is an integral over energy of I_{av}' multiplied by the effective area × solid angle of the detector. If the spectrum of the source of I_2 were that of thermal bremsstrahlung and the interstellar medium were homogeneous, then the contribution to c' from the second term in equation (6) would be proportional to the function $R_c(T, N_{\mathrm{H}})$ plotted in Figure 2. For a given temperature and column densities from 1 to 4×10^{20} cm^{-2}, this function does not deviate much from the exponential represented by the straight dashed lines drawn tangent to the semilog plots of $R_c(T, N_{\mathrm{H}})$ at $N_{\mathrm{H}} = 2 \times 10^{20}$ cm^{-2}. Without detailed calculation we shall assume that the dependence of c' on N_{H} in the case of a clumpy ISM is also approximately exponential, and that the apparent attenuation column density of c' will bear the same relation to that of $R_c(T, N_{\mathrm{H}})$ as N_{ap}' does to N_{th} in equation (4). We shall therefore write for the expectation value of the C band count rate the approximate expression

$$c' = C_1 + C_2 \exp\,[-N_{\mathrm{av}}/N_{\mathrm{ap}}(T)]\,, \tag{7}$$

where $N_{\mathrm{ap}}(T)$ is the apparent attenuation column density for C band X-rays from a source at temperature T. We assume $N_{\mathrm{ap}}(T)$ is given by equation (4) with N_{th} equal to the negative reciprocal of the natural logarithmic slope of $R_c(T, N_{\mathrm{H}})$ at $N_{\mathrm{H}} = 2.0 \times 10^{20}$ cm^{-2}. For a source temperature of $T = 10^6$ K we find $N_{\mathrm{th}} = 1.4 \times 10^{20}$ cm^{-2}. We note that this is equal to the photoelectric absorption column density for 0.22 keV X-rays.

We fitted equation (7) to each of the data sets displayed in Figure 9 by minimizing the quantity

$$Q = \frac{1}{n-3} \sum_{n=1}^{m} \frac{(c_i' - c_i)^2}{s_i^2}, \quad (8)$$

where c_i is the observed rate, and c_i' is the expectation value of the C rate in the ith cell calculated according the equation (7) with N_{av} set equal to N_i, which we call the mean value of N_H in the ith cell. The expected variance, s_i^2, was calculated according to the formula

$$s_i^2 = c_i'/t_i + (f_x c_i')^2 + [(\delta N + f_H N_i) C_2 \exp(-N_i/N_{ap})/N_{ap}]^2 . \quad (9)$$

The first term is the Poisson variance based on trial values of the parameters. The second term is the variance due to the combined effects of measurement uncertainties and intrinsic fluctuations of which one cause could be clumping of the ISM. In this term f_x represents the rms fractional fluctuation due to these effects. The third term is the variance due to measurement uncertainties in N_H. We assumed the errors in the N_H measurements due to uncertainties in the baseline determination, represented by δN, is 1.0×10^{19} cm^{-2}, and the fractional uncertainty, f_H, is 0.05. We iterated the minimizing process until trial values of C_1, C_2, N_{ap}, and f_x used in the weight factor matched the fitted values, and the minimum value of Q was 1.0. The results are tabulated in Table 3 and the fitted curves are shown in Figures 9*a*–9*h*. We see that, in general, the model accounts for the local component of the soft XRB with a C band count rate of $\sim$0.20 counts s^{-1}. The largest deviation from this value is the fit in the third octant where the best fit value is 0.267 counts s^{-1}. This elevated count rate appears to be the result of the Monoceros Gemini enhancement. If this large but spatially connected region of the sky is excluded from the fit, the number of sky cells accepted is reduced to 956, and we find values of $C_1 = 0.21$ counts s^{-1}, $C_2 = 0.44$ counts s^{-1}, and $N_{ap} = 2.25 \times 10^{20}$ cm^{-2} with $f_x = 0.111$. Thus the intensity of the local component appears to be nearly the same over the whole sky.

The best fit values of C_2 and N_{ap} differ substantially from one octant to another. We note that octant 8 contains very few data because the BTL survey scanned only a small portion of this part of the sky. The best fit values of C_2 in the other seven octants range from 0.238 to 0.657 counts s^{-1} and N_{ap} ranges from 1.22 to 5.22 $\times 10^{20}$ cm^{-2}. The fit with the least value of f_x is in the second octant defined by ($0° < b < 90°$, $90° < l < 180°$). We note that the fitted value of N_{ap} in this octant is 2.65×10^{20} cm^{-2}, which is about twice the theoretical value for 0.22 keV X-rays in uniform interstellar matter with $N_{He}/N_H = 0.085$. We believe that the poorer fits in the other octants, which are indicated by higher values of f_x and which result in generally higher values of N_{ap}, are due primarily to the presence in these other regions of more and larger foreground enhancements.

b) Subtraction of the Modeled Soft X-Ray Background from the Sky Map

We "flattened" the unsmoothed C band map by subtracting from it a map of c' values calculated according to equation (7) with globally fitted values of C_1, C_2, and N_{ap}. The same image processing technique was used as in the preparation of the original smoothed C band map except that the shading scale was adjusted to show light shade at zero counting rate. The result is shown in Figure 10. Regions which deviate positively from the two-component model appear in a darker shade and are further outlined by isointensity contours. Regions which deviate negatively from the two-component model appear at a lesser or zero shade. Since the regions of the sky which have little or no exposure are also left blank the regions of negative deviation must be distinguished by checking the exposure map of Figure 3. We note that the positive deviations from the two-component model show obvious spatial correlations, and that they appear to be emission features which now stand out more sharply.

V. DISCUSSION

a) Clumping of the Interstellar Medium

In the second octant, where the two-component model fits the data with the smallest value of f_x, we have found that the apparent attenuation column density of interstellar matter for the C band count rates is about twice the expected value. We also find that the magnitude of small-scale (2°) spatial fluctuations in the midlatitude range of this octant is 0.10. We examine now whether an explanation of the attenuation anomaly in terms of the clumping of the interstellar matter, as originally proposed by Bowyer and Field (1969) and by Bunner *et al.* (1969), is consistent with this limit on the magnitude of the spatial fluctuations and other information about the interstellar medium.

TABLE 3

BEST FIT VALUES OF THE TWO-COMPONENT MODEL PARAMETERS AND DEVIATION MEASURES FOR ALL SKY CELLS WITH MORE THAN 10 s EXPOSURE

OCTANT NO.	L_{min}, L_{max} (deg)	b_{min}, b_{max} (deg)	m	C_1 (s^{-1})	C_2 (s^{-1})	N_{ap} 10^{20} cm^{-2}	f_x
1	0, 90	0, 90	1184	0.165	0.422	3.26	0.163
2	90, 180	0, 90	924	0.167	0.438	2.65	0.134
3	180, 270	0, 90	1171	0.267	0.657	1.22	0.210
4	270, 360	0, 90	658	0.179	0.536	2.42	0.195
5	0, 90	−90, 0	1173	0.183	0.287	4.10	0.180
6	90, 180	−90, 0	802	0.178	0.328	1.52	0.190
7	180, 270	−90, 0	1024	0.221	0.238	5.22	0.230
8	270, 360	−90, 0	120	0.190	0.181	9.24	0.143
Global[a]	0, 360	−90, 90	1905	0.196	0.341	3.25	0.168

[a] All sky cells with more than 320 s exposure.

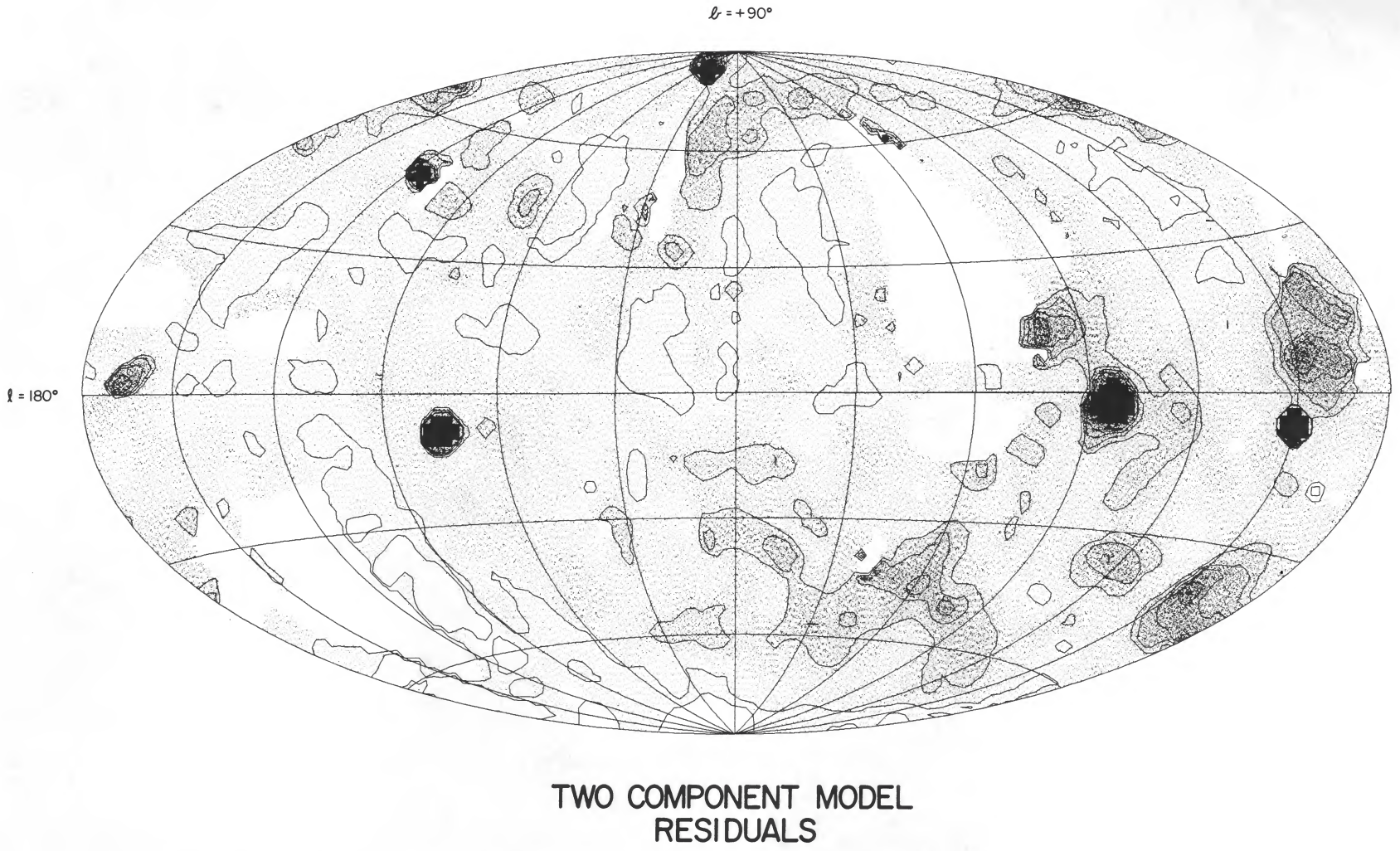

FIG. 10.—Flattened *C* band map, prepared by subtraction of a globally fitted two-component model of the soft XRB from the *C* band map shown in Fig. 5*a*. Contours are at −0.10, −0.05, 0.05, 0.10, 0.15 and 0.20 counts s^{-1}.

One can estimate the typical column density of the clumps that must be assumed to exist to explain the anomaly by solving equation (5) for N_c with $N_{ap}' = 2.0N_{th}$. The result is $N_c = 2.5 \times 10^{20}$ cm^{-2}. Numerous radio and optical studies have demonstrated the existence of interstellar clouds with column densities of this magnitude which subtend solid angles much smaller than that of our field of view. For example, Griesen (1973) found that the neutral hydrogen which produces 21 cm absorption in the continuum radio spectrum of Cas A is in clouds in the Perseus arm with a total column density between 520 and 1150 pc cm^{-3}. Griesen estimated that the number of clouds along the line of sight is between 10 and 20, which implies an average column density per cloud of about 3×10^{20} cm^{-2}. Also, he found a lack of structure on the scale of arc minutes. This is not inconsistent, however, with the existence of clumpiness on a scale small compared to the angular resolution of our survey.

Verschuur (1974) surveyed the cloud structure of 21 cm neutral hydrogen emission with a resolution of 10′ in two mid-latitude regions. His maps show typical clouds subtend a solid angle of about 1 deg^2 and have column densities of 3–5 $\times 10^{20}$ cm^{-2}. At an assumed distance of 100 pc such clouds would have a typical sizes of 2–3 pc and masses of 3–6 $M_\odot$. Such clouds satisfy the conditions required for equation (6) to be valid, namely that they subtend solid angles much less than that of the field of view.

Dickey, Salpeter, and Terzian (1977, 1978) used the Arecibo telescope (HPBW 3.′2) to measure N_H in emission at hexagonally spaced points surrounding extragalactic radio sources where N_H was measured in absorption. They identified 66 absorption features due to neutral hydrogen clouds and showed that the internal structure of these clouds is smooth on a scale of arc minutes. One can derive an upper limit to the amount of gas in these clouds by assuming that the column densities derived from 21 cm emission, seen in the same direction, are due solely to the same velocity features seen in absorption. This amounts to identifying the gas component seen in emission, but not absorption, as a warm (10^3 K) component of these clouds. The column densities so derived have averages of 1.5, 2.1, and 4.6 $\times 10^{20}$ cm^{-2} per cloud at the high, intermediate, and low latitudes, respectively.

Schwarz and Wesselius (1978) studied the 21 cm opacity distribution in front of two extended extragalactic continuum radio sources with an angular resolution of 0.′4. They found structure in the ISM on an angular scale of 0.′5–3′ corresponding to a linear scale of 0.5–3 pc, with column densities on the order of 4×10^{20} cm^{-2} and implied volume densities in the range from 42 to 253 cm^{-3}.

Hobbs (1974) deduced the statistical properties of interstellar clouds out to distances of 1.5 kpc from the Sun from optical measurements of the 7699 Å line of K I in the spectra of 17 stars. He found column densities in the range from 1.7×10^{20} to 17×10^{20} cm^{-2} with a frequency distribution that implies a space density of clouds of the form N_H^{-4} with a mean column density of 2.6×10^{20} cm^{-2}.

Thus the typical size and thickness of clouds derived from 21 cm and optical observations are consistent with the clumpiness required to explain the attenuation anomaly in the two-component model.

Given plausible values of ISM cloud parameters we can estimate the magnitude of the expected spatial fluctuations in the C band count rates due to spatial variations in the numbers of obscuring clouds. In the context of the two-component model this would appear as spatial variations in the apparent intensity of the external component. For a simple estimate we assume that there are, on the average, m completely opaque clouds of column density N_c which subtend a solid angle Ω_c within a detector field of view, Ω_d. Then m is related to the average column density, N_H, by $m = N_H \Omega_d / N_c \Omega_c$. If these clouds are distributed at random within the field of view, then the count rate of an external component will be reduced by $\exp(-m/n)$, where $n = \Omega_d/\Omega_c$. If the distribution of the number of clouds is Poisson, then $\delta m \approx m^{1/2}$. If the local and external intensities are assumed to vary slowly over the sky then from equation (7) we find

$$\frac{\delta c'}{c'} = \frac{(\Omega_c/\Omega_d)^{1/2}(N_H/N_C)^{1/2}}{1 + (C_1/C_2)\exp(N_H/N_C)} . \quad (11)$$

For $\Omega_c = 1 \times 10^{-4}$ sr (the solid angle subtended by 1 pc clouds at a distance of 100 pc), $\Omega_d = 2.1 \times 10^{-3}$ sr (the *SAS 3 C* band field of view), $N_H = 3.6 \times 10^{20}$ cm^{-2} (which is the average value at $|b| \approx 30°$; Dickey, Salpeter, and Terzian 1978), and using the globally fitted parameters C_1, C_2, $N_c \approx N_{ap}$ (Table 3) we find $\delta c'/c' = 0.08$. This estimate of the expected fluctuations is typical of the values found for the C band (Table 2). We note that the magnitude of the fluctuations which we observe does not conflict with the upper limit of 9% set by Levine *et al.* (1977) who used a detector with a field of view ~ 5 times larger than ours.

To pursue this matter further we computed the statistical properties of randomly generated simulations of the clumpy interstellar medium generated according to a model illustrated in Figure 11. We assumed Earth is at the center of a sphere of radius r filled with optically thin hot plasma which is the source of the local isotropic intensity that produces a count rate C_1. We assumed this sphere is immersed in a disk of neutral hydrogen whose mean density at height z above the central plane of the Galaxy is $n_0 \exp[-(z/h)^2]$. We assumed, further, that a fraction g of the neutral hydrogen is clumped in randomly distributed spherical clouds with uniform internal density, n_c, of neutral hydrogen and a distribution in radius, R, given by $R^{-a}dR$, with R confined to the range from R_1 to R_2. Beyond the neutral hydrogen we assumed there exists an isotropic source of the external intensity that produces a counting rate C_2 at $N_H = 0$. For a given set of these parameters we computed the expected number of clouds in the truncated cone

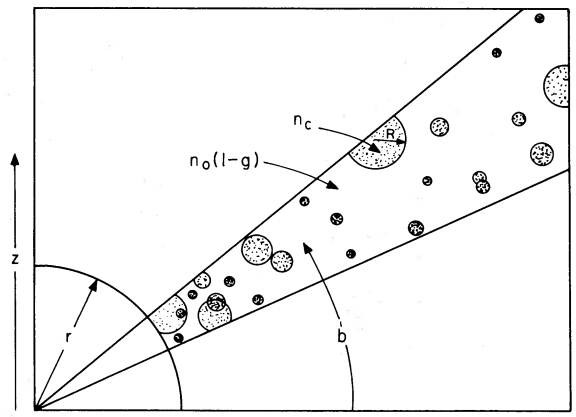

FIG. 11.—Schematic diagram of the model adopted for a Monte Carlo simulation of the clumpy interstellar medium.

defined by a 4° × 4° solid angle extending from R to infinity and centered on a specified galactic latitude. To generate one simulated map of neutral hydrogen column densities we distributed this number of clouds at random in the cone with a density of cloud centers proportional to exp $[-(z/h)^2]$. We then calculated at each point in a 100 × 100 array of points over the 4° × 4° solid angle the column density, N_H, resulting from the superposition of the clouds and the residual smoothly distributed fraction of the ISM. Figure 12*a* is an example of a map generated in this way, and Figure 12*b* shows the same map after convolution with a 10′ Gaussian beam.

For each randomly generated map we calculated the mean value, N_{av}, of the column density and the mean value, t_{av}, of the transmission, exp $(-N_H/N_{th})$, for a 1.°8 × 1.°8 map cell, taking into account the spread in the sky of the region contributing counts to the data assigned to the cell. We repeated the calculation for 100 independent 4° × 4° maps to generate a distribution of mean transmissions, and to obtain an average of the apparent attenuation lengths, which are calculated according to the formula $N_{ap} = -N_{av}/\ln(t_{av})$. We then generated 100 simulated survey maps, each consisting of 1000 pairs of exposure and counts, with exposures chosen at random with the distribution of the actual exposures of the C band map, and counts calculated as the sum of a contribution from the local intensity plus a contribution from the external intensity, reduced by a mean transmission factor chosen at random with the distribution generated as above, plus a random Poisson fluctuation. We calculated a fluctuation measure for each cell as the difference between its rate and the mean rate of the succeeding eight in the series of 1000. We then found the value, F_x, of the assumed fractional fluctuation which reduced the χ^2 value, calculated as in equation (2), to unity. Finally, we repeated the entire calculation 10 times for each set of parameters with different random numbers.

In Table 4 we list the mean value and variance of N_{ap} and F_x from the 10 trials for each of several sets of model parameters which yield values comparable to those found for the real data (see Tables 2 and 3). We note that parameter set 1 yields a satisfactory match to the real values derived for the second octant when allowance is made for the absence of measurement errors in the Monte Carlo calculations. We also list for comparison the results obtained with the parameters adopted by McKee and Ostriker (1977) in their theory of the three-component ISM.

b) Properties of the Local and External Source Plasmas

We wish now to derive the properties of source plasmas that could give rise to the components of the count rates that we identify as "local" and "external." The emission measure of a uniform source of plasma at temperature T with normal cosmic abundances which produces a given count rate, C, in our detector is

$$\mathrm{EM} = 7.9 \times 10^{-3} \frac{R_c(10^6)}{R_c(T)} C \ \mathrm{cm}^{-6} \ \mathrm{pc} , \qquad (12)$$

where $R_c(T)$ is the count rate per unit emission measure at $N_H = 0.0$ (Fig. 2).

The emission measure is related to the electron density by

$$n_e = (\mathrm{EM}/D f_f a_c)^{1/2} , \qquad (13)$$

where D is the distance through the emitting region, f_f is the filling factor, and a_c is the number of electrons per ion. The pressure in the emitting region is

$$P/k = 2 n_e T . \qquad (14)$$

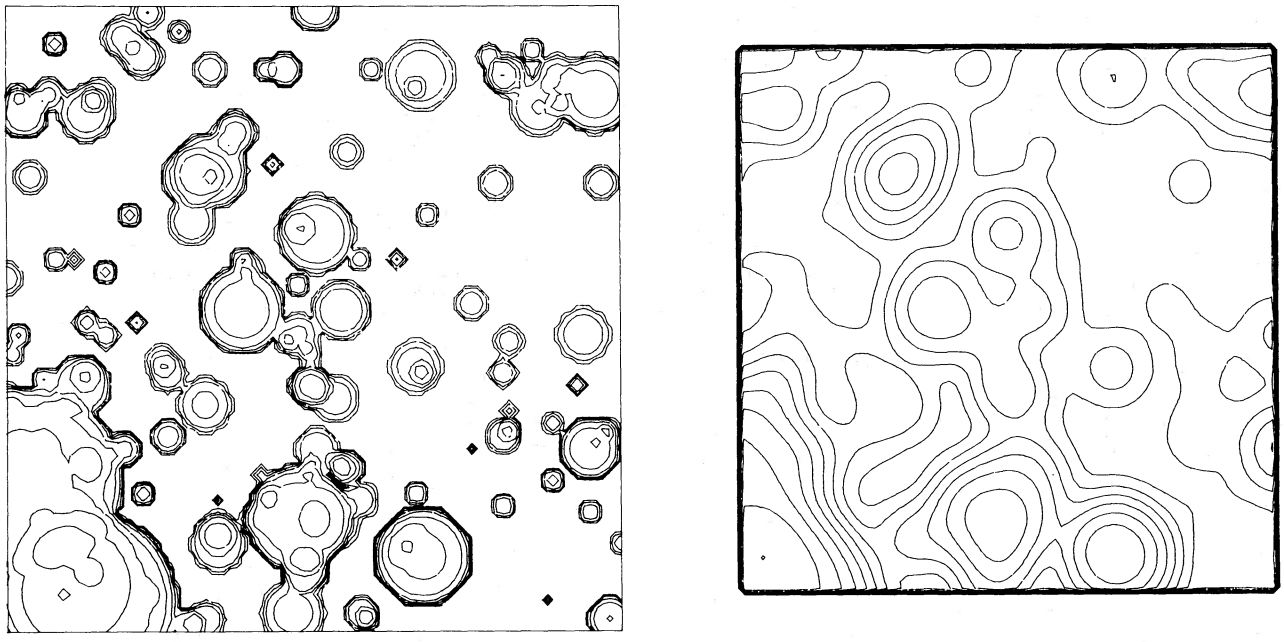

FIG. 12.—(*a*) Example of a randomly generated map of column density for the model with the no. 1 set of parameters. In this map $\langle N_H \rangle = 2.60 \times 10^{20}$ cm^{-2}, exp $(-\langle N_H \rangle/N_{th}) = 0.156$, and $\langle \exp(-N_H/N_{th}) \rangle = 0.377$. (*b*) The same map convolved with a 10′ Gaussian beam. In this map $\langle \exp(-N_H'/N_{th}) \rangle = 0.313$, where N_H' is the convolved value of the column density.

TABLE 4

APPARENT ATTENUATION COLUMN DENSITIES, N_{ap}, AND FLUCTUATION MEASURES, F_x, FOR SIMULATED SKY MAPS WITH VARIOUS SETS OF MODEL PARAMETERS

No.	b (deg)	g	n_c (cm^{-3})	a	R_1 (pc)	R_2 (pc)	N_{th} (10^{20} cm^{-2})	No. of Clouds in 4° × 4°	N_{ap} (10^{20} cm^{-2})	F_x
1	42	0.75	80	4.0	0.4	10.0	1.4	129	2.66 ± 0.09	0.084 ± 0.013
2	60	0.75	80	4.0	0.4	10.0	1.4	57	2.59 ± 0.11	0.090 ± 0.016
3	42	0.85	80	4.0	0.4	10.0	1.4	147	3.11 ± 0.12	0.097 ± 0.013
4	42	0.65	80	4.0	0.4	10.0	1.4	112	2.34 ± 0.06	0.070 ± 0.010
5	42	0.75	60	4.0	0.4	10.0	1.4	172	2.45 ± 0.08	0.088 ± 0.011
6	42	0.75	80	3.5	0.4	10.0	1.4	62	2.80 ± 0.16	0.102 ± 0.015
7	42	0.75	80	4.0	0.6	10.0	1.4	42	2.85 ± 0.10	0.095 ± 0.015
8	42	0.75	80	4.0	0.4	4.0	1.4	181	2.60 ± 0.05	0.068 ± 0.005
9	42	0.75	80	4.0	0.4	10.0	1.0	129	2.11 ± 0.08	0.072 ± 0.010
MO[a] ...	42	0.95	42	4.0	0.5	10.0	1.4	172	2.89 ± 0.08	0.138 ± 0.014

NOTE.—Fixed parameters: $r = 104$ pc; $n_0 = 0.75\,cm^{-3}$; $h = 190$ pc; $C_1 = 0.162\,s^{-1}$; $C_2 = 0.421\,s^{-1}$.
[a] McKee and Ostriker 1977.

i) *The Local Component*

From the fits of the two-component model summarized in Table 3 we conclude that the average count rate due to the local component is approximately 0.16 s^{-1}, which is the fitted value of C_1 reduced by the charged particle background rate of the detector. This corresponds to a flux of 1.4×10^{-8} ergs cm^{-2} s^{-1} sr^{-1} (0.10–0.28 keV). Stellar coronal emission is not a significant contributor to the flux in the *C* band (Tanaka and Bleeker 1977; Rosner *et al.* 1981). Our model requires that essentially all of this flux is generated in the uniform optically thin plasma of the local hot bubble. Combining equations (12), (13), and (14), and taking $a_c = 1.17$, $D = 100$ pc, and $f_f = 1.0$, we find the results shown in Figure 13 where the pressure and density are plotted as functions of the assumed temperature. The minimum pressure which these results allow is ~ 7000 cm^{-3} K which occurs in the range $(0.3–1.0) \times 10^6$ K. This pressure is several times larger than the 3200 cm^{-3} K estimated for the intercloud medium by McKee and Ostriker (1977). It is consistent with the idea (Sanders *et al.* 1977; Fried *et al.* 1980; Hayakawa *et al.* 1978; Stern and Bowyer 1979; Davelaar, Bleeker, and Deerenberg 1980; Iwan 1980) that the Sun is immersed in a local cavity of relatively high pressure, which may be the result of a supernova event.

ii) *The External Component*

We wish now to derive estimates of the emission measure and total luminosity of the source of the external component from the fitted values of the parameters of the two-component model. From Figure 2*a* it is evident that in the case of attenuation in homogeneous matter an exponential extrapolation to $N_H = 0$ of a count rate measured at $N_H = 2.0 \times 10^{20}$ cm^{-2}, represented by the straight dashed lines, would yield a value substantially less than the true unattenuated rate. This is due to the more rapid attenuation of the lower energy portion of the *C* band X-rays. For a source temperature of 10^6 K the actual rate at $N_H = 0$ is greater than the extrapolated rate by a factor of 1.6. The same effect must occur, but to a lesser extent, in the case of attenuation in clumped matter. Lacking more exact information, we shall adopt a value of 1.3 for the correction factor to convert the fitted values of C_2 to the rate at $N_H = 0$. A portion of this rate is attributable to a truly extragalactic component the spectrum of which we assume is described by an extrapolation to lower energies of the power law, $dN/dE = 7.7E^{-1.4}$ photons cm^{-2} s^{-1} sr^{-1} given by Schwartz (1978) for $1 < E < 21$ keV. We find this spectrum contributes 0.07 s^{-1} to the *C* band rates. Subtracting this we are left with 0.37 s^{-1} for the global value of the count rate due to the external component. According to the curves of Figure 2 for a plasma temperature of 10^6 K, the corresponding flux is 3.1×10^{-8} ergs cm^{-2} s^{-1} sr^{-1} (0.1–0.28 keV), the total flux is 7.1×10^{-8} ergs cm^{-2} s^{-1} sr^{-1}, and the emission measure is 2.9×10^{-3} cm^{-6} pc.

We mentioned at the outset that upper limits of a few percent have been placed on the portion of the soft XRB that originates in sources beyond nearby galactic objects on the basis of negative results from attempts to detect the effects of absorption of those objects. On the other hand, there are theoretical and observational reasons to suppose that the Galaxy has a hot corona. This idea, introduced by Spitzer (1956) and subsequently developed by many others (see York 1982 and references therein), provides a plausible explanation for the external component of the soft XRB. We examine first whether the flux we measure is consistent with the power available to heat the corona. If we assume that the global flux we find is the mean for the entire galactic disk, then the total luminosity is $L = 8\pi^2 r^2 J$, where r is the radius of the disk and J is the

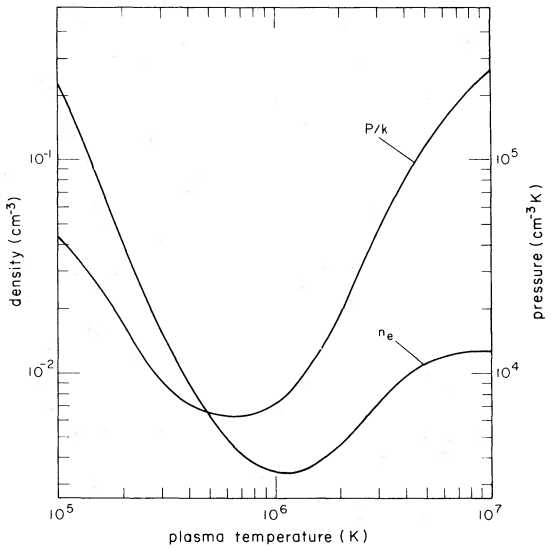

FIG. 13.—Pressure and density in the local "hot bubble" vs. temperature

average flux. Taking $r = 15$ kpc we find a luminosity of 5.4×10^{39} ergs s^{-1} (0.1–0.28 keV) and a total luminosity of 1.2×10^{40} ergs s^{-1}. McKee and Ostriker (1977) estimate a heating rate of $\sim 3 \times 10^{40}$ ergs s^{-1} due to halo supernovae. Thus halo supernovae appear to be a plausible power source for the observed flux.

The observed emission measure can also be used to estimate the density and pressure at the base of the corona. If we assume the density scale height is ~ 10 kpc (Spitzer 1956), then the scale length of the X-ray emitting region is ~ 5 kpc. The implied density and pressure at the base are $n_e = 7.6 \times 10^{-4}$ cm^{-3} and $P/k = 1.5 \times 10^3$ cm^{-3} K. We note that the implied base pressure of the corona does not exceed pressures estimated for cloud or intercloud regions in the disk of the galaxy. The mass of this corona is $3 \times 10^8 M_\odot$.

If X-ray emission from the corona of our Galaxy is detectable, one might well expect to detect coronae of other galaxies of similar type. Bregman and Glassgold (1982) used the imaging proportional counter (IPC) of the *Einstein Observatory* to image two nearby edge-on spiral galaxies, NGC 3628 and NGC 4244, and placed upper limits on diffuse emission in the energy range from 0.3 to 3 keV of 1×10^{39} and 2×10^{38} ergs s^{-1}, respectively. (We note that a 10^6 K plasma radiates ~ 0.1 times as much power in the energy range from 0.3 to 3.0 keV as in the range from 0.1 to 0.3 keV). They suggest that the supernova energy in these galaxies may be emitted at X-ray energies below the threshold of the IPC (0.4 keV) or by an ultrahot wind ($T > 10^7$ K) which radiates inefficiently. In any case, the *Einstein* results do not directly contradict the implications of a coronal interpretation of the "external" component of the *C* band rates in our own Galaxy.

c) *Deviations from the Global Two-Component Model*

Deviations from the two-component model are represented by the residual count rate map of Figure 10. Deviations of greater than 0.05 counts s^{-1} are outlined by contours. We see that the plane to pole variation of the *C* rates has been virtually eliminated by the two-component model. Deviations remain in large regions of the sky. We first note that the sources listed in Table 1 can now be seen as point-like enhancements of the *C* rates in Figure 10. One additional source of high significance appears in the flattened map at $\sim(20°, 35°)$ this is coincident with the source H1626+01 as reported by Pravdo *et al.* (1981).

Beyond the point sources, the major known *C* band enhancements as mentioned in § III*a* remain as regions of *C* rates in excess of the two-component model. Of the excesses which remain, a number occur in areas of very low N_H, ($< 1.5 \times 10^{20}$ cm^{-2}), and could be due to very soft X-ray flux from an external component, which the global parameters underestimate. These regions are seen at (70°, 45°), from (100°, 45°) to (135°, 70°), from (180°, 50°) to (180°, 70°) and at (20°, −60°). Enhancements are also seen at approximately these coordinates in the *B* band (0.130–0.188 keV) maps of McCammon *et al.* (1983) which supports the hypothesis that the excesses may be due to soft X-ray flux from the external component. One other region of excess which appears to be from a soft spectral region is at (240°, 40°). Here, too, there appears a *B* band enhancement (McCammon *et al.* 1983). The two-component model overestimates the *C* rates in several areas, the largest of which includes most of the sixth octant below $b < -30°$. The *B* band rates (McCammon *et al.* 1983) are also somewhat low in this region. Since the column densities in these regions range from 6 to 2×10^{-20} cm^{-2}, it is more likely that the deviations are due to a variation in the local component.

VI. SUMMARY AND CONCLUSIONS

1. The *C* band (0.10–0.28 keV) background X-ray intensity is anticorrelated with the column density of neutral hydrogen on all angular scales down to the angular resolution of the *SAS 3* survey (2°.9 FWHM).

2. In the octant defined by $90° < l < 180°$, $0° < b < 90°$, the *C* band and N_H survey data can be fitted well by a two-component model in which the expectation value of the *C* band count rate is related to the mean column density in the field of view by the formula $c' = C_1 + C_2 \exp(-N/N_{ap})$, with $N_{ap} = 2.7 \times 10^{20}$ cm^{-2}. The fitted value of N_{ap} is about twice the theoretical value of the absorption column density for *C* band X-rays in matter with normal cosmic abundances.

3. Spatial fluctuations in the *C* band on the scale of 2° are generally less than 10%.

4. The large value of N_{ap} can be explained as an effect of the clumping of interstellar matter in X-ray opaque clouds in a manner consistent with the observed degree of smoothness of the *C* band survey and other information about the ISM.

5. We attribute the C_1 component to X-rays produced within a local hot bubble. If the bubble is a uniform plasma out to a distance of 100 pc, then the fitted value of C_1 implies a minimum pressure of ~ 7000 cm^{-3} K at a temperature in the range from 0.3 to 1.0×10^6 K.

6. We attribute the C_2 component to X-rays produced in a galactic corona which has a luminosity in the *C* band of 5.4×10^{39} ergs s^{-1}.

7. A "flattened" *C* band map, prepared by subtraction of the rates computed according to a globally fitted two-component model, reveals foreground absorption and emission features with improved sensitivity and clarity.

David Hearn and John Richardson were responsible for the development and testing of the *SAS 3* low-energy detector system and for the development of some of the software used in the analysis. We thank them and the many others at MIT who have contributed to the *SAS 3* project. We also thank Carl Heiles for providing us with data tapes of various N_H surveys, and in particular for permission to include in our display map the BTL survey data before publication. The scientific payload for *SAS 3* was built in the Laboratory for Space Experiments at the MIT Center for Space Research; the spacecraft was developed at the Applied Physics Laboratory of the Johns Hopkins University; the project was managed by the Goddard Space Flight Center of NASA.

REFERENCES

Bowyer, C. S., and Field, G. B. 1969, *Nature*, **223**, 573.
Bowyer, C. S., Field, G. B., and Mack, J. E. 1968, *Nature*, **217**, 32.
Bregman, J. N., and Glassgold, A. E. 1982, *Ap. J.*, **263**, 564.
Brown, R. L., and Gould, R. J. 1970, *Phys. Rev. D.*, **1**, 2252.
Bunner, A. N., Coleman, P. C., Kraushaar, W. L., McCammon, D., Palmieri, T. M., Shilepsky, A., and Ulmer, M. 1969, *Nature*, **223**, 1222.
Clark, G. W. 1975, *IAU Circ.*, No. 2799.
Cleary, M. N., Heiles, C., and Haslam, C. G. T. 1979, *Astr. Ap. Suppl.*, **36**, 95.
Davelaar, J., Bleeker, J. A. M., and Deerenberg, A. J. M. 1980, *Astr. Ap.*, **92**, 231.
Davidsen, A., Shulman, S., Fritz, G., Meekins, J. F., Henry, R. C., and Friedman, H. 1972, *Ap. J.*, **177**, 629.

Dickey, J. M., Salpeter, E. E., and Terzian, Y. 1977, *Ap. J. (Letters)*, **211**, L77.
———. 1978, *Ap. J. Suppl.*, **36**, 77.
Fried, P. M., Nousek, J. A., Sanders, W. T., and Kraushaar, W. L. 1980, *Ap. J.*, **242**, 987.
Frieden, B. R. 1976, *J. Opt. Soc. America*, **66**, 280.
Gorenstein, P., and Tucker, W. H. 1976, *Ann. Rev. Astr. Ap.*, **14**, 373.
Greisen, E. W. 1973, *Ap. J.*, **184**, 363.
Hayakawa, S., Kato, T., Nagase, F., Yamashita, K., and Tanaka, Y. 1978, *Astr. Ap.*, **62**, 21.
Hearn, D. R., Marshall, F. J., and Jernigan, J. G. 1979, *Ap. J. (Letters)*, **227**, L63.
Hearn, D. R., *et al.* 1976, *Ap. J. (Letters)*, **203**, L21.
Heiles, C. 1976, *Ap. J. (Letters)*, **208**, L137.
Heiles, C., Chu, Y., Reynolds, R. J., Yegingil, I., and Troland, T. H. 1980, *Ap. J.*, **242**, 533.
Heiles, C., and Cleary, M. N. 1979, *Australian J. Phys. Ap. Suppl.*, **47**, 1.
Hobbs, L. M. 1974, *Ap. J.*, **191**, 395.
Hu, E. 1981, *Ap. J.*, **248**, 119.
Iwan, D. 1980, *Ap. J.*, **239**, 316.
Levine, A., Rappaport, S., Halpern, J., and Walter, F. 1977, *Ap. J.*, **211**, 215.
Long, K. S., Agrawal, P. C., and Garmire, G. P. 1976, *Ap. J.*, **206**, 411.
McCammon, D., Bunner, A. N., Coleman, P. L., and Kraushaar, W. L. 1971, *Ap. J. (Letters)*, **168**, L33.
McCammon, D., Burrows, D. N., Sanders, W. T., and Kraushaar, W. L. 1983, *Ap. J.*, **269**, 107.
McCammon, D., Meyer, S. S., Sanders, W. T., and Williamson, F. O. 1976, *Ap. J.*, **209**, 46.
McKee, C. F., and Ostriker, J. P. 1977, *Ap. J.*, **218**, 148.
Nugent, J. J., *et al.* 1983, *Ap. J. Suppl.*, **51**, 1.
Pravdo, S. H., Nugent, J. J., Nousek, J. A., Jensen, K. A., Wilson, A. S., and Becker, R. H. 1981, *Ap. J.*, **251**, 501.
Raymond, J. C., and Smith, B. W. 1977, *Ap. J. Suppl.*, **35**, 419.
———. 1979, private communication.
Rosner, R., *et al.* 1981, *Ap. J. (Letters)*, **249**, L5.
Sanders, W. T., Kraushaar, W. L., Nousek, J. A., and Fried, P. M. 1977, *Ap. J. (Letters)*, **217**, L87.
Schwartz, D. A. 1978, in *X-Ray Astronomy*, ed. W. A. Baity and L. E. Peterson (Oxford: Pergamon), p. 453.
Schwarz, U. J., and Wesselius, P. R. 1978, *Astr. Ap.*, **64**, 97.
Spitzer, L. 1956, *Ap. J.*, **124**, 20.
Stark, A. A., Bally, J., Linke, R., and Heiles, C. 1984, in preparation.
Stern, R., and Bowyer, S. 1979, *Ap. J.*, **230**, 755.
Tanaka, Y., and Bleeker, J. A. M. 1977, *Space Sci. Rev.*, **20**, 815.
Verschuur, G. L. 1974, *Ap. J. Suppl.*, **27**, 65.
Weaver, H. 1979, in *IAU Symposium 84, Large Scale Structure of the Galaxy*, ed. W. B. Burton (Dordrecht: Reidel), p. 295–300.
York, D. G. 1982, *Ann. Rev. Astr. Ap.*, **20**, 221.

G. W. CLARK: Room 37–611, MIT Center for Space Research, Cambridge, MA 02139

F. J. MARSHALL: Space Physics Division, Air Force Geophysics Laboratory, Hanscom AFB, Bedford, MA 01731